

Globally driven superconducting quantum computing architecture

Roberto Menta,^{1,2,*} Francesco Cioni,^{2,†} Riccardo Aiudi,¹ Marco Polini,^{1,3} and Vittorio Giovannetti^{1,2}

¹Planckian srl, I-56127 Pisa, Italy

²NEST, Scuola Normale Superiore, I-56127 Pisa, Italy

³Dipartimento di Fisica dell'Università di Pisa, Largo Bruno Pontecorvo 3, I-56127 Pisa, Italy

We propose a platform for implementing a universal, *globally driven* quantum computer based on a 2D ladder hosting three different species of superconducting qubits. In stark contrast with the existing literature, our scheme exploits the always-on longitudinal ZZ coupling. The latter, combined with specific driving frequencies, enables the reach of a blockade regime, which plays a pivotal role in the computing scheme.

Introduction. Superconducting circuits have demonstrated exceptional performance in executing precise control and measurement operations, thus making them a preferred choice for quantum computing (QC) architectures [1–7]. Nevertheless, notwithstanding their remarkable properties, these platforms are still afflicted by a serious drawback. It is indeed widely recognized that the scalability of superconducting (and other solid-state) architectures faces a hurdle because of the need for *localized* control of each logical qubit [8–11]. This challenge, often dubbed the “wiring problem”, arises from the necessity of multiple control signals for each qubit in standard QC architectures, leading to a wiring overload [1, 12, 13]. In view of this fact, maintaining high gate fidelity while scaling up the number of qubits within a single processor presents a significant hurdle [14]. While state-of-the-art superconducting QC platforms can achieve single-qubit operation fidelities as high as 99.99% [15, 16], reducing errors in two-qubit gates remains challenging. To our knowledge, the associated error rates for these operations persist at around 0.1% [17–21]. Incidentally, one of the main limiting factors to enhance two-qubit gate fidelity in superconducting platforms is the “residual” longitudinal ZZ interaction between neighboring qubits. While recent research endeavors have showcased methods to alleviate [22–25] and even leverage ZZ coupling [26–28] for implementing two-qubit gates, such interaction remains generally undesirable within conventional quantum superconducting QC frameworks.

To offer a solution to these daunting issues, we present a universal superconducting QC architecture where, exploiting the presence of always-on ZZ coupling terms, local driving of each individual qubit is replaced by *global* pulses that control *collectively* a large collection (roughly one third) of the memory registers of the model, hence drastically reducing the total number of wires necessary to run the computation. Historically, a pioneering global scheme of QC was first proposed by Lloyd [29]. Soon after, several other proposals for QC based on global control were put forward [30–32]. However, these failed to reach the readiness level necessary to be competitive with models based on local control. Our scheme is inspired by a recent disruptive advancement that was made by

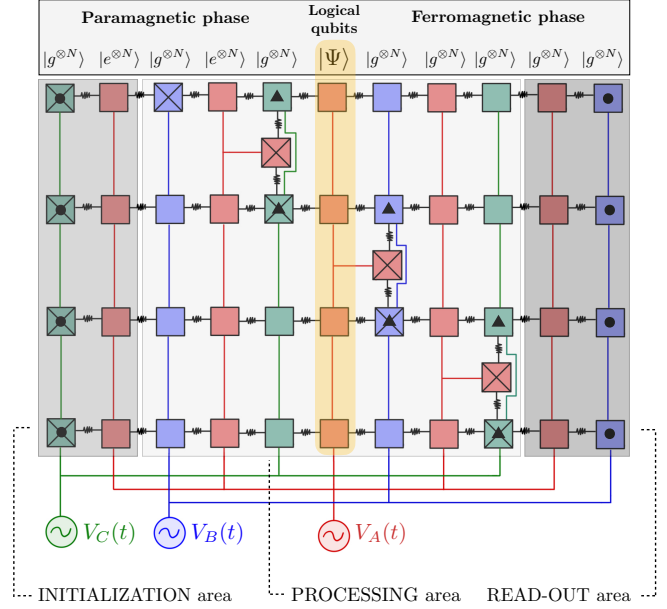


FIG. 1. Architecture for a globally driven superconducting quantum computer. Three groups, A , B , C of superconducting qubits (red, blue, and green squares, respectively) occupy the horizontal rows of a 2D ladder. Black springs, colored continuous lines, crosses, filled circles, and triangles are defined in the main text. Electrical wires depicted as continuous red, blue, and green lines connect all elements within each group, facilitating global control through independent classical electrical pulses. During the computation, the logical information is encoded in the qubits of one of the columns of the processing area (enlightened in yellow in the figure): qubits on the left (right)-hand side of such information carrier column are in a “paramagnetic” (“ferromagnetic”) geg (ggg) phase. The illustration pertains to a $N = 4$ logical qubit quantum computer.

Cesa and Pichler [33], who presented a universal quantum computer based on globally driven Rydberg atoms. In this QC platform [34, 35], two nearby atoms in an excited Rydberg state interact so strongly that their simultaneous excitation is forbidden (“Rydberg blockade” [36]). Building on this effect, the authors of Ref. [33] demonstrated that by arranging *two* different species of $\mathcal{O}(N^2)$ Rydberg atoms in an almost-regular rectangular lattice,

one can implement globally driven QC on N qubits.

Here, we propose a generalization of the results of Ref. [33] to a solid-state, superconducting platform. Readers will immediately understand that this is far from trivial since the aforementioned blockade effect does not come “for free” in our platform. Below, we show how to *dynamically* induce blockade into a lattice of superconducting qubits. Additionally, we use *three* rather than *two* species of qubits, which, as we argue below, significantly reduces (with respect to Ref. [33]) the number of physical qubits that are needed to implement a universal quantum computer. Last but not least, we propose a different initialization scheme with respect to that of Ref. [33], which helps us reducing the size of the initialization area of our solid-state quantum computer with respect to the Rydberg one. In our model, quantum information is always localized in the N superconducting qubits of one of the vertical columns that form the lattice (see Fig. 1), referred to as the “information carrier column” (ICC) in the following, while the remaining qubits are kept in a reference (separable) configuration. Quantum computation proceeds through sequences of control pulses that operate collectively on one or more of three species of qubits. These pulses serve to rigidly shift the position of the ICC in the ladder and activate single- and two-qubit gates on its elements at specific locations in the device, both enabled by the *blockade interactions* that connect the qubits. In our device, such interactions are implemented via the unwanted ZZ coupling mentioned above. As we will discuss below, by exploiting the fact that ZZ interactions can alleviate some of the degeneracies in the energy spectra of neighboring superconducting qubits, we selectively impede specific energy transitions, effectively emulating Rydberg blockade [33] on a superconducting platform.

Model. We propose the quantum computing architecture depicted in Fig. 1, which consists of a 2D ladder with N parallel rows. The ladder contains $2N + 3$ columns, each housing a distinct type of superconducting qubits chosen among three possible species A , B , and C (represented, respectively, by red, blue, and green squares in the figure), organized in the

$$\underbrace{CABA}_{\text{row 1}} \underbrace{CABA}_{\text{row 2}} \underbrace{CABA}_{\text{row 3}} \dots \quad (1)$$

pattern. The first (last) two columns on the left (right) boundary of the ladder serve as dedicated areas for the initialization (read-out) stage of quantum computation. The central portion of the scheme, encompassing $2N - 1$ columns, represents instead the processing area of the model where the quantum computation takes place. In this area, starting from the third column, each of the B - and C -type columns also incorporates an additional A -type qubit. This A -type qubit acts as a “coupler” between adjacent rows of the ladder, enabling two-qubit logic gates [37]. All qubits within a group share the

same level spacing: $\hbar\omega_A$ for A -type qubits, $\hbar\omega_B$ for B -type qubits, and $\hbar\omega_C$ for C -type qubits. Exceptions to this rule, marked with a black circle or triangle in Fig. 1, have level spacings slightly detuned from the nominal values to compensate for the “anomalous” (i.e., different) number of nearest-neighboring ZZ interacting elements (see the next paragraphs for details). In our model, qubits within the same row are interconnected via nearest-neighbor ZZ coupling, with uniform strength $\hbar\zeta$, depicted as black springs in the figure. This interaction also links additional intrarow coupler A -type qubits with adjacent B or C elements in the same column. Crucially, all A -type qubits are collectively driven by a *single* time-dependent external electrical signal, $V_A(t)$, via a continuous red line. Similarly, all B -type [C -type] qubits, including those with a black circle or triangle, are collectively driven by signal $V_B(t)$ [$V_C(t)$] through a dedicated blue [green] line. Finally, the crossed qubits in the device identify a subset of superconducting qubits A , B , or C that, while maintaining their nominal level spacings, couple with the external electrical signals $V_A(t)$, $V_B(t)$, or $V_C(t)$ at augmented Rabi frequencies. As shown in the figure, crossed elements of the same type never appear in the same row or column. Additionally, the pattern (1) ensures that any two columns that contain crossed elements of the same type B or C are always separated by a sequence of *three* columns that contain no crossed qubits of that same type. We point out that this feature, which is crucial for implementing single-qubit and two-qubit gates, can be engineered *at the level of circuit fabrication* and needs no extra control (see the Supplemental Material, SM [38]).

The total Hamiltonian of the ladder in Fig. 1 can be written as $\hat{H}(t) := \hat{H}_0 + \hat{H}_{\text{drive}}(t)$, where

$$\hat{H}_0 := \sum_{\chi \in \{A, B, C\}} \sum_{i \in \chi} \frac{\hbar\omega_i}{2} \hat{\sigma}_i^{(z)} + \sum_{\langle i, j \rangle} \frac{\hbar\zeta}{2} \hat{\sigma}_i^{(z)} \otimes \hat{\sigma}_j^{(z)} \quad (2)$$

describes the local energy contribution of the superconducting qubits and their always-on ZZ interactions, while

$$\hat{H}_{\text{drive}}(t) := \sum_{\chi \in \{A, B, C\}} \sum_{i \in \chi} \hbar\Omega_\chi(t) \sin(\omega_{d,\chi}t + \phi_\chi(t)) \hat{\sigma}_i^{(y)} \quad (3)$$

represents the time-dependent driving owing to the classical control lines.

In Eqs. (2) and (3), $\hat{\sigma}_i^{(x,y,z)}$ represent the Pauli matrices acting on the Hilbert space of the i th qubit, expressed in the local energy basis $|g_i\rangle := (0, 1)^T$, $|e_i\rangle := (1, 0)^T$. The summation in the second term on the right-hand side of Eq. (2) runs over all nearest-neighbor qubits. The parameter $\omega_{d,\chi}$ denotes the oscillation frequency of the driving pulse $V_\chi(t)$, while $\Omega_\chi(t)$ and $\phi_\chi(t)$ define the time-dependent Rabi frequency and phase of such control. For simplicity, in writing Eq. (2), we have not specified that when i identifies a blue [green] qubit with a black circle,

addressing of both regular and crossed qubits using only global pulses.

Following Ref. [33], we encode the quantum information on the 2D ladder by placing one logical qubit per row. As indicated in Fig. 1, at each computational step, these qubits reside on a single column of the processing area of the device. Such ICC can be formed either by A -, B -, or C -type qubits. However, if the ICC is formed by B - or C -type qubits, the red-crossed elements in Fig. 1, which act as intrarow couplers, are not involved in the encoding but will always remain into the ground state $|g\rangle$ of their local Hamiltonian.

The ICC is positioned at the interface between two strings of qubits: a “ferromagnetic” phase ($|gggg\dots\rangle$) on the right, and a “paramagnetic” phase ($|\dots gegeg\rangle$) on the left. Assuming that at a given computational step a (possibly entangled) state $|\Psi\rangle$ of the N -logical qubit is located in the k th column of the ladder, the global quantum state of the model is described by *well-formed* vectors of the form

$$|\Psi; k\rangle := \left(\dots |g^{\otimes N}\rangle_{k-3} \otimes |e^{\otimes N}\rangle_{k-2} \otimes |g^{\otimes N}\rangle_{k-1} \right) \otimes |\Psi\rangle_k \otimes \left(|g^{\otimes N}\rangle_{k+1} \otimes |g^{\otimes N}\rangle_{k+2} \otimes |g^{\otimes N}\rangle_{k+3} \dots \right), \quad (7)$$

where, for $k = 1, \dots, 2N + 3$, the ket $|\dots\rangle_k$ refers to the state of the k -th column of the device. As shown in the SM [38], starting from a fully ferromagnetic phase, where all the qubits of the device are in the ground state $|g\rangle$, a specific control pulse $V_C(t)$ can promote the first C -type column of the initialization area of Fig. 1 in $|e^{\otimes N}\rangle$. Formally, this produces a vector $|\Psi; k\rangle$ where the ICC is located in the first B -type column of the processing area, and a logical state $|\Psi\rangle := |g^{\otimes N}\rangle$. Thanks to Eq. (7), one can show that, under e - e blockade conditions, there exist control unitary evolutions (5) that enable universal QC. The key ingredients that make this feasible are: (a) the ability to *rigidly* move the ICC at any position in the ladder (including the last column of the read-out area where measurements can be performed at the end of the computation); (b) the possibility to implement arbitrary single-qubit gates on the crossed element of the B - or C -type column where the ICC is located, while leaving the rest of the qubits unaffected; and (c) the ability to activate a nontrivial two-qubit entangling gate (e.g., a control- Z operation) between the j th and $(j + 1)$ th logical qubits when the ICC is located in the B - or C -type column that contains the crossed A -type qubit, which acts as a coupler between the j th and $(j + 1)$ th rows of the ladder.

To achieve task (a), we identify a sequence \hat{U}_{shift} [43] of transformations (6) that shifts the horizontal position of the ICC without affecting its internal state, i.e., $\hat{U}_{\text{shift}}|\Psi; k\rangle = |\Psi; k + 1\rangle$, see Fig. 2(b).

In the case in which the ICC is located in a χ -type column with $\chi \in \{B, C\}$, the operations needed

for implementing the single-qubit gates of point (b) can be realized by composing sequences of the form $\hat{Z}_{A^r}^{\text{tot}} \hat{W}_{\chi \times}(\theta/2, -\mathbf{n}_\perp) \hat{Z}_{A^r}^{\text{tot}} \hat{W}_{\chi \times}(\theta/2, \mathbf{n}_\perp)$ with \mathbf{n}_\perp orthogonal to \mathbf{z} and $\hat{Z}_{A^r}^{\text{tot}}$ obtained from (6) for $\theta' = 2\pi$ and $\theta'' = 0$ (see the [38]). Indeed, thanks to the fact that the crossed χ -type qubits are located on columns, which are at least three columns apart from each other, when acting on $|\Psi; k\rangle$ the above transformation will effectively correspond to the application of the single-qubit rotation $\hat{\mathbb{R}}(\theta, \mathbf{n}_\perp)$ on the crossed element of the ICC [44]. Finally, once the ICC is aligned with a two-qubit gate, we only need to use a single $\hat{Z}_{A^r}^{\text{tot}}$ evolution obtained by setting $\theta' = 0$ and $\theta'' = 2\pi$ in Eq. (6), which leaves unchanged every regular A -type qubit and induces conditional-phase shift [42] on the crossed ones.

Discussion. Exploiting ZZ interactions, we achieved universal QC on N logical qubits through external *global* pulses that act on a ladder of $N_{\text{tot}} = 2N^2 + 4N - 1$ physical qubits [37]. In contrast with the Rydberg-atom proposal [33], which relies on the use of two different species of physical qubits, our scheme uses three species. This choice allows us to roughly halve the total number of physical qubits of the device, which for the two-species model [33] scales as $N_{\text{tot}} \simeq 4N^2$ for $N \gg 1$. As discussed above, the condition $\eta_{\text{BR}} \gg 1$ is crucial for our device’s operation. Numerical checks in the SM [38] confirm that ζ must be at least on the order of $5\Omega_\chi$. The largest values of ζ that have been experimentally achieved [45] are on the order of 100 MHz, while typical Rabi frequencies can reach values as small as 5 MHz [46], suggesting that the blockade regime is fully within reach in current superconducting-qubit platforms.

In order to achieve a fault-tolerant quantum computation, error-correction (EC) schemes are necessary. Since our machine is universal, any standard fault-correction procedure can be implemented. In particular, regarding, e.g., surface codes [47] or qLDPC codes [48, 49], we mention that while our proposal uses only nearest-neighbor couplings, nothing prevents us from introducing long-range couplings between logical qubits in order to reach 2D connectivity requirements. This can be experimentally carried out, for example, by following the approaches of Refs. [50, 51]. We finally mention that existing EC schemes for globally controlled quantum computers have been studied in the past [52–56]; however, globally driven EC codes for our machine will be subject of future research. Moreover, a significant challenge of our architecture is the impact of inhomogeneities in SC qubit frequencies and coupling strengths on protocol fidelity. Although a detailed noise analysis is beyond the scope of this Letter, we remark that systematic fabrication errors could be treated as standard dynamical errors within error correcting schemes, as shown in Ref. [57], thus allowing the strategies discussed above to be applied. An alternative strategy involves a *hybrid* “bottom-up mitigation approach”, where global control

is applied to small qubit patches or chiplets (with fabrication inhomogeneities below a set tolerance). These patches will be then connected to each other [58, 59]. For instance, suppose that in order to have N logical qubits, we need to build k patches with inhomogeneities below the above mentioned tolerance, each encoding M logical qubits. For each patch we have $\mathcal{O}(1)$ control lines. By coupling the k chiplets we still have $\mathcal{O}(k)$ wires with $k \sim N/M$. This configuration would still significantly reduce the number of control lines required for universal QC. The calculation of the tolerance required is left for future work. Another potential challenge is that qubit state readout is currently limited to the rightmost column of the ladder, complicating the individual qubit tune-up typically required for gate calibration. To address this, flip-chip technology could be employed, for example by coupling the computational chip to a top readout chip that performs individual readout of the qubits inside the ladder [60].

Acknowledgments. We thank F. Cesa and M. Riccardi for useful discussions, and J. Despres for useful comments on the draft. This work has been funded by the European Union - NextGenerationEU, Mission 4, Component 2, under the Italian Ministry of University and Research (MUR) Extended Partnership PE00000023 National Quantum Science and Technology Institute – NQSTI – CUP J13C22000680006.

M.P. and V.G. are co-founders and shareholders of Planckian. At the time of their contributions, authors affiliated with Planckian are either employees at Planckian or PhD students collaborating with Planckian.

* rmenta@planckian.co; These authors contributed equally to this work.

† francesco.cioni@sns.it; These authors contributed equally to this work.

- [1] J. M. Gambetta, J. M. Chow, and M. Steffen, Building logical qubits in a superconducting quantum computing system, *npj Quantum Inf.* **3**, 2 (2017).
- [2] F. Arute, K. Arya, R. Babbush, D. Bacon, J. C. Bardin, R. Barends, R. Biswas, S. Boixo, F. G. S. L. Brandao, D. A. Buell, *et al.*, Quantum supremacy using a programmable superconducting processor, *Nature* **574**, 505 (2019).
- [3] M. Kjaergaard, M. E. Schwartz, J. Braumüller, P. Krantz, J. IJ. Wang, S. Gustavsson, and W. D. Oliver, Superconducting qubits: Current state of play, *Annu. Rev. Condens. Matter Phys.* **11**, 369 (2020).
- [4] A. Blais, A. L. Grimsmo, S. M. Girvin, and A. Wallraff, Circuit quantum electrodynamics, *Rev. Mod. Phys.* **93**, 025005 (2021).
- [5] Y. Wu, W.-S. Bao, S. Cao, F. Chen, M.-C. Chen, X. Chen, T.-H. Chung, H. Deng, Y. Du, D. Fan, *et al.*, Strong quantum computational advantage using a superconducting quantum processor, *Phys. Rev. Lett.* **127**, 180501 (2021).
- [6] S. Bravyi, O. Dial, J. M. Gambetta, D. Gil, and Z. Nazario, The future of quantum computing with superconducting qubits, *J. Appl. Phys.* **132**, 160902 (2022).
- [7] O. Ezratty, Perspective on superconducting qubit quantum computing, *Eur. Phys. J. A* **59**, 94 (2023).
- [8] J. Q. You and F. Nori, Superconducting circuits and quantum information, *Phys. Today* **58**(11), 42 (2005).
- [9] R. J. Schoelkopf and S. M. Girvin, Wiring up quantum systems, *Nature (London)* **451**, 664 (2008).
- [10] M. H. Devoret and R. J. Schoelkopf, Superconducting circuits for quantum information: An outlook, *Science* **339**, 1169 (2013).
- [11] G. Wendin, Quantum information processing with superconducting circuits: A review, *Rep. Prog. Phys.* **80**, 106001 (2017).
- [12] H. Mukai, K. Sakata, S. J. Devitt, R. Wang, Y. Zhou, Y. Nakajima, and J.-S. Tsai, Pseudo-2D superconducting quantum computing circuit for the surface code: Proposal and preliminary tests, *New J. Phys.* **22**, 043013 (2020).
- [13] S. Kwon, A. Tomonaga, G. L. Bhai, S. J. Devitt, and J.-S. Tsai, Gate-based superconducting quantum computing, *J. Appl. Phys.* **129**, 041102 (2021).
- [14] E. J. Zhang, S. Srinivasan, N. Sundaresan, D. F. Bogorin, Y. Martin, J. B. Hertzberg, J. Timmerwilke, E. J. Pritchett, J.-B. Yau, C. Wang, *et al.*, High-performance superconducting quantum processors via laser annealing of transmon qubits, *Sci. Adv.* **8**, eabi6690 (2022).
- [15] Z. Li, P. Liu, P. Zhao, Z. Mi, H. Xu, X. Liang, T. Su, W. Sun, G. Xue, J.-N. Zhang, *et al.*, Error per single-qubit gate below 10^{-4} in a superconducting qubit, *npj Quantum Inf.* **9**, 111 (2023).
- [16] A. Somoroff, Q. Ficheux, R. A. Mencia, H. Xiong, R. Kuzmin, and V. E. Manucharyan, Millisecond coherence in a superconducting qubit, *Phys. Rev. Lett.* **130**, 267001 (2023).
- [17] R. Barends, *et al.*, Diabatic gates for frequency-tunable superconducting qubits, *Phys. Rev. Lett.* **123**, 210501 (2019).
- [18] B. Foxen, C. Neill, A. Dunsworth, P. Roushan, B. Chiaro, A. Megrant, J. Kelly, Z. Chen, K. Satzinger, *et al.* (Google AI Quantum), Demonstrating a continuous set of two-qubit gates for near-term quantum algorithms, *Phys. Rev. Lett.* **125**, 120504 (2020).
- [19] S. Krinner, P. Kurpiers, B. Royer, P. Magnard, I. Tsitsilin, J. C. Besse, A. Remm, A. Blais, and A. Wallraff, Demonstration of an all-microwave controlled-phase gate between far-detuned qubits, *Phys. Rev. Appl.* **14**, 044039 (2020).
- [20] L. Ding, M. Hays, Y. Sung, B. Kannan, J. An, A. Di Paolo, A. H. Karamlou, T. M. Hazard, K. Azar, *et al.*, High-fidelity, frequency-flexible two-qubit fluxonium gates with a transmon coupler, *Phys. Rev. X* **13**, 031035 (2023).
- [21] A. P. Singh, K. Mitarai, Y. Suzuki, K. Heya, Y. Tabuchi, K. Fujii, and Y. Nakamura, Experimental demonstration of a high-fidelity virtual two-qubit gate, *Phys. Rev. Res.* **6**, 0132350 (2024).
- [22] J. Ku, X. Xu, M. Brink, D. C. McKay, J. B. Hertzberg, M. H. Ansari, and B. L. T. Plourde, Suppression of unwanted ZZ interactions in a hybrid two-qubit system, *Phys. Rev. Lett.* **125**, 200504 (2020).
- [23] Z. Ni, S. Li, L. Zhang, J. Chu, J. Niu, T. Yan, X. Deng, L. Hu, J. Li, Y. Zhong, S. Liu, F. Yan, Y. Xu, and D. Yu,

- Scalable method for eliminating residual ZZ interaction between superconducting qubits, *Phys. Rev. Lett.* **129**, 040502 (2022).
- [24] X. Xu and M. H. Ansari, ZZ freedom in two-qubit gate, *Phys. Rev. Appl.* **15**, 064074 (2021).
- [25] Z. Huang, T. Kim, T. Roy, Y. Lu, A. Romanenko, S. Zhu, and A. Grassellino, Fast ZZ-free entangling gates for superconducting qubits assisted by a driven resonator, *Phys. Rev. Appl.* **22**, 034007 (2024).
- [26] M. C. Collodo, J. Herrmann, N. Lacroix, C. K. Andersen, A. Remm, S. Lazar, J.-C. Besse, T. Walter, A. Wallraff, and C. Eichler, Implementation of conditional phase gates based on tunable ZZ interactions, *Phys. Rev. Lett.* **125**, 240502 (2020).
- [27] P. Zhao, P. Xu, D. Lan, J. Chu, X. Tan, H. Yu, and Y. Yu, High-contrast ZZ interaction using superconducting qubits with opposite-sign anharmonicity, *Phys. Rev. Lett.* **125**, 200503 (2020).
- [28] J. Long, T. Zhao, M. Bal, R. Zhao, G. S. Barron, H.-s. Ku, J. A. Howard, X. Wu, C. Rae H. McRae, X.-H. Deng, *et al.*, A universal quantum gate set for transmon qubits with strong ZZ interactions, [arXiv:2103.12305](https://arxiv.org/abs/2103.12305).
- [29] S. Lloyd, A potentially realizable quantum computer, *Science* **261**, 1569 (1993).
- [30] S. C. Benjamin, Schemes for parallel quantum computation without local control of qubits, *Phys. Rev. A* **61**, 020301 (2000).
- [31] S. C. Benjamin, Quantum computing without local control of qubit-qubit interactions, *Phys. Rev. Lett.* **88**, 017904 (2001).
- [32] S. C. Benjamin and S. Bose, Quantum computing with an always-on Heisenberg interaction, *Phys. Rev. Lett.* **90**, 247901 (2003).
- [33] F. Cesa and H. Pichler, Universal quantum computation in globally driven Rydberg atom arrays, *Phys. Rev. Lett.* **131** 170691, (2023).
- [34] For an excellent review on quantum information with Rydberg atoms see e.g. M. Saffman, T. G. Walker, and K. Mølmer, Quantum information with Rydberg atoms, *Rev. Mod. Phys.* **82**, 2313 (2010).
- [35] C. Fromonteil, R. Tricarico, F. Cesa, and H. Pichler, Hamilton-Jacobi-Bellman equations for Rydberg-blockade processes, *Phys. Rev. Res.* **6**, 033333 (2024).
- [36] E. Urban, T. A. Johnson, T. Henage, L. Isenhower, D. D. Yavuz, T. G. Walker, and M. Saffman, Observation of Rydberg blockade between two atoms, *Nat. Phys.* **5**, 110 (2009).
- [37] The total number of row-couplers is equal to $N - 1$, bringing the total number of superconducting qubits to $N_{\text{tot}} = (2N + 3)N + N - 1 = 2N^2 + 4N - 1$, while the total number of columns is $N_{\text{column}} = 2N + 3$.
- [38] See the Supplemental Material for a wealth of additional technical details.
- [39] More specifically at any given time, either the control pulse $V_A(t)$ is active while $V_B(t)$ and $V_C(t)$ are not, or, if either $V_B(t)$ or $V_C(t)$ is active, then $V_A(t)$ is not i.e. $\Omega_A(t) \neq 0 \Rightarrow \Omega_B(t) = \Omega_C(t) = 0$, and $\Omega_B(t) \neq 0$ or $\Omega_C(t) \neq 0 \Rightarrow \Omega_A(t) = 0$.
- [40] Depending on the circuit design, indeed, the longitudinal ZZ-coupling ζ in Eq. (2) can be either positive [22, 24, 27, 28] or negative [23, 26]. However, its sign does not influence the blockade effect. Indeed, the ZZ interaction detunes the $|eg\rangle \rightarrow |ee\rangle$ and $|ge\rangle \rightarrow |ee\rangle$ transitions with respect to the non-interacting case, effectively “blocking” these transitions and making the $|ee\rangle$ state inaccessible with the external pulses that we use. Also, we remark that $\zeta \sim \text{kHz} - \text{MHz}$ while the natural frequency of the qubits is $\omega_\chi \sim \text{GHz}$. Thus, for a two-qubit system, the $|ee\rangle$ state is the highest in energy even in the presence of interactions.
- [41] Here, the symbol $\bar{\chi}$ denotes a species that is distinct from χ .
- [42] M. A. Nielsen and I. L. Chuang, *Quantum Computation and Quantum Information* (Cambridge University Press, Cambridge, 2010).
- [43] This can be done through three different types of π pulses: one that acts only on the non-crossed elements of A [i.e. $\hat{\Pi}_{A^r} := \hat{W}_{A^r}(\pi, \mathbf{x})$], and the others on the full set of B - and C -type qubits [i.e. $\hat{\Pi}_B := \hat{W}_B(\pi, \mathbf{x}; \pi, \mathbf{x})$, $\hat{\Pi}_C := \hat{W}_C(\pi, \mathbf{x}; \pi, \mathbf{x})$]. Specifically, if the ICC of $|\Psi; k\rangle$ is of B or C type, we take $\hat{U}_{\text{shift}} = \hat{\Pi}_{A^r} \hat{\Pi}_B \hat{\Pi}_C \hat{\Pi}_{A^r}$, while if it is of A type we use $\hat{U}_{\text{shift}} = \hat{\Pi}_B \hat{\Pi}_C \hat{\Pi}_{A^r} \hat{\Pi}_B \hat{\Pi}_C$. Notice that, since in both scenarios the action of \hat{U}_{shift} on the well-formed state coincides (up to a global phase) with its own inverse (see the SM [38]), the same operation can also be used to induce a collective motion of the interface in the opposite direction, i.e., $\hat{U}_{\text{shift}}|\Psi; k+1\rangle = |\Psi; k\rangle$, see Fig. 2(b).
- [44] The key observation here is that when the k th column of $|\Psi; k\rangle$ is made of B -type qubits, the unitary $\hat{Z}_{A^r}^{\text{tot}}$ defined at the end of the previous section is equivalent to the application of a $\hat{\sigma}^{(z)}$ gate to each of the element of the ICC, i.e., $\hat{Z}_{A^r}^{\text{tot}}|\Psi; k\rangle = \left(\hat{\sigma}^{(z)}\right)^{\otimes N}|\Psi; k\rangle$. Notably, the same property holds also when we replace the $|g^{\otimes N}\rangle$ state of a ferromagnetic B -type column of $|\Psi; k\rangle$ with a generic N -qubit state. Exploiting this effect it then follows that, given a unit vector \mathbf{n}_\perp orthogonal to \mathbf{z} , the sequence $\hat{Z}_{A^r}^{\text{tot}} \hat{W}_{B^\times}(\theta/2, -\mathbf{n}_\perp) \hat{Z}_{A^r}^{\text{tot}} \hat{W}_{B^\times}(\theta/2, \mathbf{n}_\perp)$ maps $|\Psi; k\rangle$ into a new state $|\Psi'; k\rangle$ with a new ICC vector $|\Psi'\rangle$ obtained from $|\Psi\rangle$ via the application of the single-qubit rotation $\hat{\sigma}^{(z)} \hat{\mathbb{R}}(\theta/2, -\mathbf{n}_\perp) \hat{\sigma}^{(z)} \hat{\mathbb{R}}(\theta/2, \mathbf{n}_\perp) = \hat{\mathbb{R}}(\theta, \mathbf{n}_\perp)$ on the crossed element of the column. Analogous considerations apply also to the case in which the ICC is of C type.
- [45] L. DiCarlo, J. M. Chow, J. M. Gambetta, L. S. Bishop, B. R. Johnson, D. I. Schuster, J. Majer, A. Blais, L. Frunzio, S. M. Girvin, and R. J. Schoelkopf, Demonstration of two-qubit algorithms with a superconducting quantum processor, *Nature* **460**, 240 (2009).
- [46] Y. Sung, A. Vepsäläinen, J. Braumüller, F. Yan, J. I.-J. Wang, M. Kjaergaard, R. Winik, P. Krantz, A. Bengtsson, A. J. Melville, *et al.*, Multi-level quantum noise spectroscopy, *Nat. Commun.* **12**, 967 (2021).
- [47] A. G. Fowler, M. Mariantoni, J. M. Martinis, and A. N. Cleland, Surface codes: Towards practical large-scale quantum computation, *Phys. Rev. A* **86**, 032324 (2024).
- [48] J. Roffe, D. R. White, S. Burton, and E. Campbell, Decoding across the quantum low-density parity-check code landscape, *Phys. Rev. Res.* **2**, 043423 (2020).
- [49] N. P. Breuckmann and J. N. Eberhardt, Quantum low-density parity-check codes, *PRX Quantum* **2**, 040101 (2021).
- [50] F. Marxer, A. Vepsäläinen, S. W. Jolin, J. Tuorila, A. Landra, C. Ockeloen-Korppi, W. Liu, O. Aho, A. Auer, L. Belzane, *et al.*, Long-distance transmon coupler with cz-gate fidelity above 99.8%, *PRX Quantum* **4**, 010314 (2023).

- [51] X. Deng, W. Zheng, X. Liao, H. Zhou, Y. Ge, J. Zhao, D. Lan, X. Tan, Y. Zhang, S. Li, and Y. Yu, Long-range ZZ interaction via resonator-induced phase in superconducting qubits, [arXiv:2408.16617](#).
- [52] A. Bririd, S. C. Benjamin, and A. Kay, Quantum error correction in globally controlled arrays, [arXiv:quant-ph/0308113](#).
- [53] A. Kay, Error correcting the control unit in global control schemes, [arXiv:quant-ph/0504197](#).
- [54] A. Kay, Deriving a fault-tolerant threshold for a global control scheme, [arXiv:quant-ph/0702239](#).
- [55] J. Fitzsimons, and J. Twamley, Globally controlled fault tolerant quantum computation, [arXiv:0707.1119](#).
- [56] J. Fitzsimons, and J. Twamley, Quantum fault tolerance in systems with restricted control, *Electronic Notes in Theor. Computer Sci.* **258**, 35 (2009).
- [57] D. Aharonov, and M. Ben-Or, Fault-tolerant quantum computation with constant error rate, *SIAM J. Comput.* **38**, 4 (2008).
- [58] A. Gold, J. P. Paquette, A. Stockklauser, M. J. Reagor, M. S. Alam, A. Bestwick, N. Didier, A. Nersisyan, F. Oruc, A. Razavi, *et al.*, Entanglement across separate silicon dies in a modular superconducting qubit device, *npj Quantum Inf* **7**, 142 (2021).
- [59] J. Niu, L. Zhang, Y. Liu, J. Qiu, W. Huang, J. Huang, H. Jia, J. Liu, Z. Tao, W. Wei, *et al.*, Low-loss interconnects for modular superconducting quantum processors, *Nat. Electron.* **6**, 235–241 (2023).
- [60] D. Rosenberg, D. Kim, R. Das, D. Yost, S. Gustavsson, D. Hover, P. Krantz, A. Melville, L. Racz, G. O. Samach, *et al.*, 3D integrated superconducting qubits, *npj Quantum Inf* **3**, 42 (2017).

Supplemental Material for: “Globally driven superconducting quantum computing architecture”

Roberto Menta,^{1,2} Francesco Cioni,² Riccardo Aiudi,¹ Marco Polini,^{1,3} and Vittorio Giovannetti^{1,2}

¹*Planckian srl, I-56127 Pisa, Italy*

²*NEST, Scuola Normale Superiore, I-56127 Pisa, Italy*

³*Dipartimento di Fisica dell'Università di Pisa, Largo Bruno Pontecorvo 3, I-56127 Pisa, Italy*

In this Supplemental Material file we provide additional technical details in order to clarify the results presented in the main text. In Section I, we briefly summarize well-known facts about superconducting qubits and their control via external classical drivings. We also discuss how to couple two superconducting qubits via the longitudinal ZZ coupling and how such interaction, in addition to off-resonance pulses, can induce the e - e blockade regime discussed in the main text. We also briefly recap available experimental paths to realize ZZ interactions, as available in the literature. In Section II we solve the dynamical evolution of the ladder in the rotating frame, deep in the e - e blockade regime. In particular, we provide an explicit derivation of Eq. (6) in the main text. In Section III we present a detailed analysis of how to perform universal quantum computation in our architecture. Finally, in Section IV we present basic numerical simulations of our pulsed protocol for globally-driven universal quantum computation.

I. FUNDAMENTALS OF SUPERCONDUCTING QUBITS

In this Section, with the sole aim of producing a self-contained document, we briefly recap textbook fundamentals of superconducting qubits.

A superconducting qubit [S1, S2] is a superconducting circuit that can be effectively described as a two-level system. The Hamiltonian is

$$\hat{H}_0 = \frac{\hbar\omega_\chi}{2} \hat{\sigma}^{(z)}, \quad (1)$$

where $\chi = A, B, C$ denotes the qubit type, $\hat{\sigma}^{(z)}$ is the Pauli- z operator and $\omega_\chi = (E_e - E_g)/\hbar$ is the energy splitting between the excited $|e\rangle := (1, 0)^T$ and ground state $|g\rangle := (0, 1)^T$ of the qubit. The magnitude of ω_χ depends only on the geometric parameters of the quantum chip. Indeed, for a simple qubit design as the one shown in Fig. 1, the frequency is given by $\omega_\chi = (\sqrt{8E_J E_C} - E_C)/\hbar$ where $E_C = e^2/(2C_\Sigma)$ is the total charging energy, $C_\Sigma = C_s + C_J$ is the total capacitance, including the shunt capacitance C_s and the self-capacitance of the junction C_J , while $E_J = I_c \Phi_0/2\pi$ is the Josephson energy, with I_c being the critical current of the junction and $\Phi_0 = h/(2e)$ being the superconducting magnetic flux quantum. It turns out that there are some kind of superconducting qubits known as *split transmons* (SQUID), which enable frequency tunability using externally applied magnetic field [S1]. By connecting the χ -type superconducting qubit to an external electric potential source $V_\chi(t)$, as shown in Fig. 1, we are able to perform unitary rotations on the qubit. Here we outline how this is achieved. Following the connection with the external classical source, we introduce an additional interaction term in the Hamiltonian, i.e.

$$\hat{H}_{\text{drive},\chi}(t) = \mathcal{V} V_\chi(t) \hat{\sigma}^{(y)}, \quad (2)$$

where $\mathcal{V} := (C_d/C_\Sigma) \sqrt{\hbar/(2\sqrt{L_J/C_s})}$ is a constant depending on the construction parameters of the circuit. Here, L_J is the inductance associated to the Josephson Junction. We can generally assume that the time-dependent part of the voltage takes a generic oscillatory form,

$$V_\chi(t) = \mathcal{S}_\chi(t) \sin(\omega_{d,\chi} t + \phi_\chi(t)), \quad (3)$$

where $\omega_{d,\chi}$ is the fundamental frequency of the driving pulse, $\mathcal{S}_\chi(t)$ is an envelope function, and finally $\phi_\chi(t)$ is the phase of the driving that in the following we shall assume to be time-dependent. It is instructive to move into a frame rotating with the drive frequency $\omega_{d,\chi}$. This is done by defining the unitary operator $\hat{U}_{\text{rf}}(t) = \exp(i\omega_{d,\chi} \hat{\sigma}^{(z)} t/2)$ such that the new state in the rotating frame is $|\psi_{\text{rf}}(t)\rangle = \hat{U}_{\text{rf}}(t) |\psi(t)\rangle$. The time-evolution in this new frame is given by the Schrödinger equation,

$$i\hbar \frac{\partial}{\partial t} |\psi_{\text{rf}}(t)\rangle = \left(\underbrace{i\hbar \dot{\hat{U}}_{\text{rf}}(t) \hat{U}_{\text{rf}}^\dagger(t) + \hat{U}_{\text{rf}}(t) \hat{H}_0 \hat{U}_{\text{rf}}^\dagger(t)}_{\hat{H}'_0} + \underbrace{\hat{U}_{\text{rf}}(t) \hat{H}_{\text{drive},\chi}(t) \hat{U}_{\text{rf}}^\dagger(t)}_{\hat{H}'_{\text{drive},\chi}(t)} \right) |\psi_{\text{rf}}(t)\rangle. \quad (4)$$

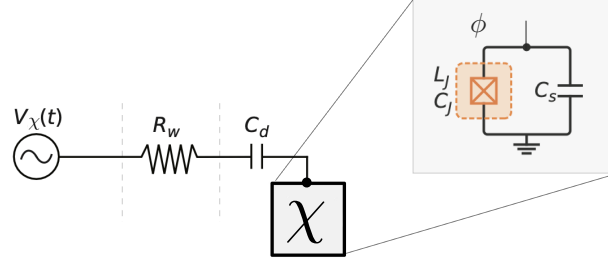


FIG. 1: Superconducting qubit driven by an external electric potential $V_\chi(t)$. For a crossed superconducting qubit (refer to Fig. 1 in the main text), the driving capacitance is doubled compared to normal χ -type qubits, i.e. $C_d \rightarrow 2C_d$, resulting in $\Omega_\chi \rightarrow 2\Omega_\chi$. That is essential for implementing quantum gates in our architecture.

Simple manipulations show that in this frame we have $\hat{H}'_0 = \hbar\Delta_\omega\hat{\sigma}^{(z)}/2$, where $\Delta_\omega = \omega_\chi - \omega_{d,\chi}$ is the detuning. The driving term instead yields

$$\begin{aligned} \hat{H}'_{\text{drive},\chi}(t) &= \mathcal{V}V_\chi(t)(\cos(\omega_{d,\chi}t)\hat{\sigma}^{(y)} + \sin(\omega_{d,\chi}t)\hat{\sigma}^{(x)}) \\ &= \hbar\Omega_\chi(t)\sin(\omega_{d,\chi}t + \phi_\chi(t))(\cos(\omega_{d,\chi}t)\hat{\sigma}^{(y)} + \sin(\omega_{d,\chi}t)\hat{\sigma}^{(x)}) \\ &= \hbar\Omega_\chi(t)\left(\frac{e^{i(\omega_{d,\chi}t + \phi_\chi(t))} - e^{-i(\omega_{d,\chi}t + \phi_\chi(t))}}{2i}\right)\left(\frac{e^{-i\omega_{d,\chi}t}(\hat{\sigma}^{(y)} + i\hat{\sigma}^{(x)}) + e^{i\omega_{d,\chi}t}(\hat{\sigma}^{(y)} - i\hat{\sigma}^{(x)})}{2}\right) \\ &= \hbar\Omega_\chi(t)\left(\frac{e^{i(\omega_{d,\chi}t + \phi_\chi(t))} - e^{-i(\omega_{d,\chi}t + \phi_\chi(t))}}{2}\right)(e^{-i\omega_{d,\chi}t}|g\rangle\langle e| - e^{i\omega_{d,\chi}t}|e\rangle\langle g|), \end{aligned}$$

with $\Omega_\chi(t) := \mathcal{V}S_\chi(t)/\hbar$ the time-dependent Rabi frequency. Notice that $\Omega_\chi(t)$ depends on \mathcal{V} , which itself depends on the capacitance coupling the qubit and the driving source. This allows us to change C_d and consequently \mathcal{V} in order to modify the time-independent part of the Rabi frequency. This procedure is the one adopted to realize crossed qubits (see the main text). Performing the multiplication and dropping fast rotating terms that will approximately average to zero (i.e. terms with $2\omega_{d,\chi}$), known as rotating wave approximation (RWA), the Hamiltonian $\hat{H}'_{\text{drive},\chi}$ can be written as

$$\hat{H}'_{\text{drive},\chi}{}^{(\text{RWA})}(t) = \frac{\hbar\Omega_\chi(t)}{2}\left(e^{i\phi_\chi(t)}|g\rangle\langle e| + e^{-i\phi_\chi(t)}|e\rangle\langle g|\right), \quad (5)$$

which allows Rabi transitions between the ground and the excited states and vice-versa.

A. The ZZ coupling implies the blockade regime

In this Section, we show that in the rotating frame induced by the unitary transformation $\hat{U}_{\text{rf}}(t) := \bigotimes_i e^{i\hat{\sigma}_i^{(z)}\omega_{d,i}t/2}$, the Hamiltonian $\hat{H}(t)$ of the 2D ladder, under RWA reduces to $\hat{H}_{\text{rf}}(t)$ of Eq. (4) of the main text. Following the approach detailed in the previous Section moving in the rotating frame we have

$$\hat{H}_{\text{rf}}(t) = \underbrace{i\hbar\dot{\hat{U}}_{\text{rf}}(t)\hat{U}_{\text{rf}}^\dagger(t) + \hat{U}_{\text{rf}}(t)\hat{H}_0\hat{U}_{\text{rf}}^\dagger(t)}_{\hat{H}'_0} + \underbrace{\hat{U}_{\text{rf}}(t)\hat{H}_{\text{drive}}(t)\hat{U}_{\text{rf}}^\dagger(t)}_{\hat{H}'_{\text{drive}}(t)}, \quad (6)$$

with \hat{H}'_0 and $\hat{H}'_{\text{drive}}(t)$ being the many-body Hamiltonians described in Eqs. (2) and (3) of the main text which we express here as

$$\hat{H}'_0 = \sum_i \frac{\hbar\omega_i}{2}\hat{\sigma}_i^{(z)} + \sum_{\langle i,j \rangle} \frac{\hbar\zeta}{2}\hat{\sigma}_i^{(z)} \otimes \hat{\sigma}_j^{(z)}, \quad (7)$$

$$\hat{H}'_{\text{drive}}(t) = \sum_i \hbar\Omega_\chi(t)\sin(\omega_{d,\chi}t + \phi_\chi(t))\hat{\sigma}_i^{(y)}, \quad (8)$$

without explicitly stating which type of qubit is associated with the i -th qubit, but maintain the convention that if the index happens to identify a regular χ -type qubit then $\omega_i = \omega_\chi$, if instead identifies a χ -type qubit with a black circle then $\omega_i = \omega_\chi^\bullet := \omega_\chi - \zeta$, and finally if it identifies a χ -type qubit with a black triangle then $\omega_i = \omega_\chi^\blacktriangle := \omega_\chi + \zeta$.

Notice hence that despite the presence of the ZZ couplings one has $\hat{U}_{\text{rf}}(t)\hat{H}_0\hat{U}_{\text{rf}}^\dagger(t) = \hat{H}_0$ and that $i\hbar\dot{\hat{U}}_{\text{rf}}(t)\hat{U}_{\text{rf}}^\dagger(t) = -\sum_i \frac{\hbar\omega_{d,i}}{2}\hat{\sigma}_i^{(z)}$. Accordingly the first contribution of Eq. (6) can be expressed as

$$\hat{H}'_0 := \frac{\hbar}{2} \left(\sum_i (\omega_i - \omega_{d,i})\hat{\sigma}_i^{(z)} + \sum_{\langle i,j \rangle} \zeta \hat{\sigma}_i^{(z)} \otimes \hat{\sigma}_j^{(z)} \right). \quad (9)$$

Observe next that by imposing $\omega_{d,\chi} = \omega_\chi - 2\zeta$, in the rotating frame the frequencies of the qubits becomes proportional to the number of ZZ connections they share with their neighbouring qubits, i.e.

$$\begin{cases} \omega_\chi^\bullet - \omega_{d,\chi} = (\omega_\chi - \zeta) - (\omega_\chi - 2\zeta) = \zeta & \text{(one connection),} \\ \omega_\chi - \omega_{d,\chi} = \omega_\chi - (\omega_\chi - 2\zeta) = 2\zeta & \text{(two connections),} \\ \omega_\chi^\blacktriangle - \omega_{d,\chi} = (\omega_\chi + \zeta) - (\omega_\chi - 2\zeta) = 3\zeta & \text{(three connections).} \end{cases} \quad (10)$$

Accordingly we can rewrite (9) as a sum of triples of the form

$$\hat{H}'_0 = \frac{\hbar\zeta}{2} \sum_{\langle i,j \rangle} \left(\hat{\sigma}_i^{(z)} + \hat{\sigma}_i^{(z)} \otimes \sigma_j^{(z)} + \sigma_j^{(z)} \right) = \hbar 2\zeta \sum_{\langle i,j \rangle} |e_i e_j\rangle \langle e_i e_j| + \text{const.} \quad (11)$$

where in the last passage we used the identity

$$\begin{aligned} \hat{\sigma}_i^{(z)} + \hat{\sigma}_i^{(z)} \otimes \sigma_j^{(z)} + \sigma_j^{(z)} &= 3|e_i e_j\rangle \langle e_i e_j| - |e_i g_j\rangle \langle e_i g_j| - |g_i e_j\rangle \langle g_i e_j| - |g_i g_j\rangle \langle g_i g_j| \\ &= 4|e_i e_j\rangle \langle e_i e_j| + \text{const.} \end{aligned} \quad (12)$$

The driving term of Eq. (6) instead yields

$$\begin{aligned} \hat{H}'_{\text{drive}}(t) &= \sum_i \hbar\Omega_\chi(t) \sin(\omega_{d,\chi}t + \phi_\chi(t)) \left(\cos(\omega_{d,\chi}t) \hat{\sigma}_i^{(y)} + \sin(\omega_{d,\chi}t) \hat{\sigma}_i^{(x)} \right) \\ &= \sum_i \hbar\Omega_\chi(t) \left(\frac{e^{i(\omega_{d,\chi}t + \phi_\chi(t))} - e^{-i(\omega_{d,\chi}t + \phi_\chi(t))}}{2i} \right) \left(\frac{e^{-i\omega_{d,\chi}t} (\hat{\sigma}_i^{(y)} + i\hat{\sigma}_i^{(x)}) + e^{i\omega_{d,\chi}t} (\hat{\sigma}_i^{(y)} - i\hat{\sigma}_i^{(x)})}{2} \right) \\ &= \sum_i \hbar\Omega_\chi(t) \left(\frac{e^{i(\omega_{d,\chi}t + \phi_\chi(t))} - e^{-i(\omega_{d,\chi}t + \phi_\chi(t))}}{2} \right) \left(e^{-i\omega_{d,\chi}t} |g_i\rangle \langle e_i| + e^{i\omega_{d,\chi}t} |e_i\rangle \langle g_i| \right), \end{aligned} \quad (13)$$

which under RWA becomes

$$\hat{H}'_{\text{drive}}(t) \simeq \hat{H}'_{\text{drive}}(\text{RWA})(t) := \sum_i \frac{\hbar\Omega_\chi(t)}{2} \left(e^{i\phi_\chi(t)} |g_i\rangle \langle e_i| + e^{-i\phi_\chi(t)} |e_i\rangle \langle g_i| \right). \quad (14)$$

Replacing (11) and (14) into Eq. (6) gives Eq. (4) of the main text.

B. Realizations of ZZ coupling

Our architecture relies on superconducting qubits that interact with their neighbors via a ZZ coupling. In modern quantum architectures, this kind of interaction is exploited to implement C-Phase gates and it has been already investigated in numerous experiments, using different strategies. In this Section, we present three of the possible ways this interaction can be realized.

1. Cavity mediated coupling

One way to reach an effective ZZ interaction between two superconducting qubits is to connect them dispersively through a cavity, i.e. a waveguide whose resonance frequency is detuned with respect to the one of the qubits. This was experimentally demonstrated in Ref. [S3], where they reached a ZZ interaction of magnitude 160 MHz. Such coupling can be obtained starting from the usual Tavis-Cummings Hamiltonian of two qubits interacting with the same cavity. In the dispersive regime, where the cavity is far detuned with respect to the qubits, one can show that

the cavity degrees of freedom can be eliminated via a Schrieffer-Wolff transformation. The result is an effective ZZ interaction of strength

$$\zeta = -2g_A^2 g_B^2 \left(\frac{1}{\delta_A \Delta_B^2} + \frac{1}{\delta_B \Delta_A^2} + \frac{1}{\Delta_A \Delta_B^2} + \frac{1}{\Delta_A^2 \Delta_B} \right), \quad (15)$$

where $\Delta_\chi = \omega_{01}^{(\chi)} - \omega_c$, $\delta_\chi = \omega_{01}^{(\chi)} - \omega_{12}^{(\chi)}$, with $\omega_{jk}^{(\chi)}$ being the level spacing between the states with j and k excitation for the χ -type qubit with $\chi = A, B$; g_A and g_B correspond to the couplings between the corresponding qubit and the waveguide. The main issue of this scheme is that the cavity gives also rise to a SWAP interaction (of the type $\hat{\sigma}_+^{(A)} \hat{\sigma}_-^{(B)} + \hat{\sigma}_+^{(B)} \hat{\sigma}_-^{(A)}$) between the qubits. However, this can be neglected if one consider the qubits far detuned from each other.

2. Qubit mediated coupling: Josephson junctions directly connected

Another possibility for realizing the ZZ coupling is to place a third superconducting qubits (called coupler) that mediates the interaction between the two qubits. The coupler can be placed such that the Josephson junctions of the three qubits are directly connected to each other. The main advantage of this architecture is that it provides the ability to make the SWAP interaction vanishing for a certain coupler frequency. This scheme was implemented experimentally in Ref. [S4] and studied numerically in Ref. [S5]. The interaction engineered in this way depends on the circuit elements as

$$\zeta = -\frac{E_J^c E_C}{8\hbar E_J}, \quad (16)$$

with E_J and E_C being respectively the Josephson and charge energy of the qubits and E_J^c the Josephson energy of the coupler. Only small couplings have so far been measured (< 10 MHz), but numerical calculations hint at the possibility of engineering stronger interactions up to 300 MHz, while at the same time keeping the SWAP interaction close to zero. However, this relies on a coupler qubit having a very low Josephson energy (20 MHz), which might not be feasible experimentally. Moreover, it could be challenging to scale this approach to a large number of qubits as the system becomes increasingly sensitive to flux noise, as it was pointed out in Ref. [S6].

3. Qubit mediated coupling: Josephson junctions capacitively connected

The last strategy we briefly mention here is similar to the cavity-mediated approach, but using a qubit instead of a waveguide to mediate the coupling. The difference with the second approach we presented is that in this case the three qubits interacts capacitively, and are not physically coupled. In order to compute the effective ZZ interaction between the qubits, one has to perform two Schrieffer-Wolff transformations. The first transformation is needed to eliminate the degrees of freedom of the coupler and it is allowed when the qubits are detuned with respect to it. The second one can be performed when the two qubits are detuned with respect to each other, and it is needed to eliminate the SWAP term. The effective ZZ coupling was calculated up to fourth order in Refs. [S7, S8]. The first non-zero contribution for the coupling strength is approximately given by

$$\zeta \approx -\frac{g^2(\alpha_A + \alpha_B)}{(\Delta_{AB} + \alpha_A)(\Delta_{AB} - \alpha_B)}, \quad (17)$$

with $\Delta_{AB} = \omega_A - \omega_B$ is the detuning between the two qubits, α_χ is the anharmonicity of the χ -type qubit and g is the capacitive coupling between the qubits and the coupler. This scheme was investigated experimentally in Ref. [S9], where they reached a coupling strength of ~ 50 MHz, and numerically in Ref. [S6]. It is worth mentioning that this type of building block is the one employed in modern quantum architectures, e.g. in the Sycamore quantum processor [S10].

II. DYNAMICAL EVOLUTION OF THE 2D LADDER

In this Section we discuss in details the dynamical evolution of the 2D ladder. The material is organized as follows: in Sec. II A we solve the equation of motion for arbitrary sequences of control pulses under the e - e blockade regime proving that they allows us to realize a certain product of the operators $\hat{W}_\chi(\theta', \mathbf{n}'; \theta'', \mathbf{n}'')$ defined in Eq. (6) of the

main text; in Sec. II B we present some generic properties of control unitaries $\hat{W}_\chi(\theta', \mathbf{n}'; \theta'', \mathbf{n}'')$; in Sec. II C we finally show that any possible transformations $\hat{W}_\chi(\theta', \mathbf{n}'; \theta'', \mathbf{n}'')$ can be implemented by properly selecting the sequences of our global controls.

A. Effective dynamics under e - e blockade conditions

As detailed in the main text, in our model the classical control functions $\Omega_\chi(t)$ and $\phi_\chi(t)$ associated with the pulses $V_A(t)$, $V_B(t)$, and $V_C(t)$ assume constant values on disjoint time intervals. More precisely, in our analysis we assume that if $V_A(t)$ is active (not null), than both $V_B(t)$ and $V_C(t)$ must be null, and vice-versa that if either $V_B(t)$ or $V_C(t)$ or both are active, than $V_A(t)$ must be null, i.e.

$$\begin{cases} V_A(t) \neq 0 \implies V_B(t) = V_C(t) = 0, \\ V_B(t) \neq 0 \implies V_A(t) = 0, \\ V_C(t) \neq 0 \implies V_A(t) = 0, \end{cases} \quad (18)$$

(notice that $V_B(t)$ and $V_C(t)$ are allowed to act on the system at the same time). Formally this implies that we can divide the temporal evolution into a collection of disjoint time windows $\mathcal{T}_1, \mathcal{T}_2, \dots, \mathcal{T}_\ell$ where the Hamiltonian $\hat{H}_{\text{rf}}(t)$ of Eq. (4) of the main text can be treated as time-independent, i.e.

$$\hat{H}_{\text{rf}}(t) = \hat{H}_{\text{rf}}^{(\ell)} := \sum_{\chi \in X_\ell} \sum_{i \in \chi} \frac{\hbar \Omega_\chi^{(\ell)}}{2} \left(e^{i\phi_\chi^{(\ell)}} |g_i\rangle \langle e_i| + \text{H.c.} \right) + \sum_{\langle i, j \rangle} 2\hbar \zeta |e_i e_j\rangle \langle e_i e_j|, \quad \forall t \in \mathcal{T}_\ell, \quad (19)$$

where X_ℓ is the subset of $\{A, B, C\}$ that specifies which controls are active in the ℓ -th time interval, and where, given $\chi \in X_\ell$, $\Omega_\chi^{(\ell)}$ and $\phi_\chi^{(\ell)}$ are the constant values assumed by the functions $\Omega_\chi(t)$ and $\phi_\chi(t)$ on such interval, respectively. Notice that from (18) it follows that the only allowed possibility for X_ℓ are $\{A\}$ (A -type qubit controlled, B - and C -type not), $\{B\}$ (B -type qubit controlled, A - and C -type qubit not), $\{C\}$ (C -type qubit controlled, A - and B -type qubit not), and finally $\{B, C\}$ (B - and C -type qubit controlled, A -type qubit not). Therefore the total evolution induced by $\hat{H}_{\text{rf}}(t)$ can be expressed as the sequence in Eq. (5) of the main text, i.e.

$$\hat{U}_{\text{tot}} := \overleftarrow{\text{exp}} \left[-\frac{i}{\hbar} \int_{\mathcal{T}_{\text{tot}}} dt' \hat{H}_{\text{rf}}(t') \right] = \hat{U}^{(\ell)} \dots \hat{U}^{(2)} \hat{U}^{(1)}, \quad (20)$$

where $\overleftarrow{\text{exp}}[\dots]$ stands for the time-ordered exponential, $\mathcal{T}_{\text{tot}} := \mathcal{T}_1 \cup \mathcal{T}_2 \cup \dots \cup \mathcal{T}_\ell$ is the total time interval of the dynamics, and

$$\hat{U}^{(\ell)} := \exp \left[-\frac{i}{\hbar} \hat{H}_{\text{rf}}^{(\ell)} \tau_\ell \right], \quad (21)$$

is the unitary evolution associated with the ℓ -th time interval (τ_ℓ being its temporal duration). In the e - e blockade regime where the coupling constant ζ is the main energy scale of the model (i.e. $\eta_{\text{BR}} := |\zeta/\Omega_\chi^{(\ell)}| \gg 1$), the transitions induced by the driving part of $\hat{H}_{\text{rf}}^{(\ell)}$ are suppressed whenever they involve input or final states where at least one of the interacting neighbours of the χ -type qubits affected by the control is in the excited state. More precisely we shall see that in the limit $\eta_{\text{BR}} \gg 1$ each element $\hat{U}^{(\ell)}$ of the sequence (20) can be expressed in terms of control unitary gates of the form

$$\hat{U}_\chi^{(\ell)} := \prod_{i \in \chi} \left[\hat{\mathbf{1}}_i \otimes \hat{Q}_{\langle i \rangle} + \hat{U}_i^{(\ell)} \otimes \hat{P}_{\langle i \rangle} \right], \quad (22)$$

up to a global unitary gate that can be postponed to the very end of the process and which plays no role in the process. In Eq. (22) $\hat{P}_{\langle i \rangle}$ is the projector on the subspace of the nearest-neighbouring qubits of the i -th qubit which contains no excitations, $\hat{Q}_{\langle i \rangle}$ is the orthogonal complement of $\hat{P}_{\langle i \rangle}$, while finally $\hat{U}_i^{(\ell)}$ is the single-qubit unitary evolution induced by the Rabi contribution of the Hamiltonian $\hat{H}_{\text{rf}}^{(\ell)}$ on the χ -type qubits, i.e.

$$\hat{U}_i^{(\ell)} := \exp \left[-i \frac{\Omega_\chi^{(\ell)} \tau_\ell}{2} \left(e^{i\phi_\chi^{(\ell)}} |g_i\rangle \langle e_i| + \text{H.c.} \right) \right] = \exp \left[-i \frac{\Omega_\chi^{(\ell)} \tau_\ell}{2} \left(\cos(\phi_\chi^{(\ell)}) \hat{\sigma}_i^{(x)} + \sin(\phi_\chi^{(\ell)}) \hat{\sigma}_i^{(y)} \right) \right]. \quad (23)$$

We recall that if the index i identifies a regular (possibly crossed) χ -type qubit we have $\hat{P}_{\langle i \rangle} := |gg\rangle\langle gg|$ and $\hat{Q}_{\langle i \rangle} := |ee\rangle\langle ee| + |eg\rangle\langle eg| + |ge\rangle\langle ge|$, where $|gg\rangle$, $|eg\rangle$, $|ge\rangle$, $|ee\rangle$, represent the energy levels of the two qubits that exhibit a ZZ coupling with such qubit (notice that in case the i -th qubit is of B - or C - type, then such qubits will be always of A -type; while if the i -th qubit is of A -type, then they can be of B - or C -type). On the contrary if i identifies a B or a C qubit with a black circle then, the qubit is coupled with only a single A -type qubit so that $\hat{P}_{\langle i \rangle} := |g\rangle\langle g|$ and $\hat{Q}_{\langle i \rangle} := |e\rangle\langle e|$. Finally if instead i identifies a B -type or a C -type qubit with a black triangle then there are three interacting A -type qubits so that $\hat{P}_{\langle i \rangle} := |ggg\rangle\langle ggg|$ and $\hat{Q}_{\langle i \rangle} := |eee\rangle\langle eee| + |eeg\rangle\langle eeg| + \dots + |gge\rangle\langle gge|$. To prove Eq. (22) it is convenient to express the unitary (21) in the interaction picture, identifying the interaction part \hat{H}_{int} of the Hamiltonian (19) with the term that is proportional to the Rabi frequency, and the free-contribution \hat{H}_{free} with the term that is instead proportional to the ZZ coupling, i.e.

$$\hat{H}_{\text{rf}}^{(\ell)} = \hat{H}_{\text{free}} + \hat{H}_{\text{int}}^{(\ell)}, \quad \begin{cases} \hat{H}_{\text{free}} := \sum_{\langle i,j \rangle} 2\hbar\zeta |e_i e_j\rangle\langle e_i e_j|, \\ \hat{H}_{\text{int}}^{(\ell)} := \sum_{\chi \in X_\ell} \sum_{i \in \chi} \frac{\hbar\Omega_\chi^{(\ell)}}{2} \left(e^{i\phi_\chi^{(\ell)}} |g_i\rangle\langle e_i| + \text{H.c.} \right). \end{cases} \quad (24)$$

Accordingly we can then write

$$\hat{U}^{(\ell)} = \exp \left[-\frac{i}{\hbar} \hat{H}_{\text{rf}}^{(\ell)} \tau_\ell \right] = \exp \left[-\frac{i}{\hbar} \hat{H}_{\text{free}} \tau_\ell \right] \overleftarrow{\exp} \left[-\frac{i}{\hbar} \int_{\mathcal{T}_\ell} dt' \hat{H}_{\text{int}}^{(\ell)}(t') \right], \quad (25)$$

where τ_ℓ is the duration of the time window \mathcal{T}_ℓ and

$$\hat{H}_{\text{int}}^{(\ell)}(t) := \exp \left[\frac{i}{\hbar} \hat{H}_{\text{free}} t \right] \hat{H}_{\text{int}}^{(\ell)} \exp \left[-\frac{i}{\hbar} \hat{H}_{\text{free}} t \right], \quad (26)$$

the interaction term expressed in the interaction picture. To determine $\hat{H}_{\text{int}}^{(\ell)}(t)$ observe that the various contributions of \hat{H}_{free} all commute so that we can write

$$e^{-\frac{i}{\hbar} \hat{H}_{\text{free}} t} = \prod_{\langle i,j \rangle} e^{-i\zeta |e_i e_j\rangle\langle e_i e_j| t} = \prod_{\langle i,j \rangle} \left(\hat{\mathbb{1}}_{ij} + (e^{-i\zeta t} - 1) |e_i e_j\rangle\langle e_i e_j| \right), \quad (27)$$

where $\hat{\mathbb{1}}_{ij}$ is the identity operator on the Hilbert space of the i -th and j -th qubit that form an interacting ZZ couple $\langle i, j \rangle$. Observe also that when acting on a generic product state $|\vec{J}\rangle$ of the ladder qubits formed by elements of the computational basis $\{|g\rangle, |e\rangle\}$ (e.g. states of the form $|e_1 g_1 e_2 e_3 \dots g_M\rangle$ with M being the total number of qubit in the system), the transformation $e^{-\frac{i}{\hbar} \hat{H}_{\text{free}} t}$ will evolve it by adding a phase contribution $e^{-i\zeta t}$ for each of the ZZ interacting couples which are in the $|ee\rangle$ configuration. More explicitly we can write

$$e^{-\frac{i}{\hbar} \hat{H}_{\text{free}} t} |\vec{J}\rangle = e^{-iM(\vec{J})\zeta t} |\vec{J}\rangle, \quad (28)$$

with $M(\vec{J})$ the integer that counts the number of ZZ interacting couples which in the sequence $|\vec{J}\rangle$ are in the $|ee\rangle$ state. To see how $e^{-\frac{i}{\hbar} \hat{H}_{\text{free}} t}$ transforms \hat{H}_{int} it is useful to recall that the $|g_i\rangle\langle e_i|$ which enters in Eq. (24) is an operator on the full ladder, that for all qubits but the i -th, acts as the identity. In particular, indicating with $|\vec{J}^{(i)}\rangle$ a generic element of the computational basis $\{|g\rangle, |e\rangle\}$ of the entire collection of the qubits of the system excluded the i -th we can write

$$|g_i\rangle\langle e_i| \equiv \sum_{\vec{J}^{(i)}} |g_i \vec{J}^{(i)}\rangle\langle e_i \vec{J}^{(i)}|. \quad (29)$$

From Eq. (28) it hence follows that

$$e^{\frac{i}{\hbar} \hat{H}_{\text{free}} t} |g_i\rangle\langle e_i| e^{-\frac{i}{\hbar} \hat{H}_{\text{free}} t} = \sum_{\vec{J}^{(i)}} e^{-i[M_g(\vec{J}^{(i)}) - M_e(\vec{J}^{(i)})]\zeta t} |g_i \vec{J}^{(i)}\rangle\langle e_i \vec{J}^{(i)}|, \quad (30)$$

with $M_g(\vec{J}^{(i)})$ and $M_e(\vec{J}^{(i)})$ counting respectively the number of ZZ interacting couples which in the sequences $|g_i \vec{J}^{(i)}\rangle$ and $|e_i \vec{J}^{(i)}\rangle$ are in the $|ee\rangle$ state. Observe that by construction we have that $M_e(\vec{J}^{(i)})$ is always greater than or equal

to $M_g(\vec{J}^{(i)})$, and that the two coincide if and only if the qubits with which the i -th qubits are ZZ-coupled, are all in the ground state, a condition which can be expressed as

$$\begin{cases} \hat{Q}_{(i)}|\vec{J}^{(i)}\rangle = |\vec{J}^{(i)}\rangle & \implies M_e(\vec{J}^{(i)}) \geq M_g(\vec{J}^{(i)}) + 1, \\ \hat{P}_{(i)}|\vec{J}^{(i)}\rangle = |\vec{J}^{(i)}\rangle & \implies M_e(\vec{J}^{(i)}) = M_g(\vec{J}^{(i)}), \end{cases} \quad (31)$$

with $\hat{P}_{(i)}$ and $\hat{Q}_{(i)}$ the projectors appearing in Eq. (22). Accordingly we can write

$$\begin{aligned} e^{\frac{i}{\hbar}\hat{H}_{\text{free}}t}|g_i\rangle\langle e_i|e^{-\frac{i}{\hbar}\hat{H}_{\text{free}}t} &= \sum_{\vec{J}^{(i)}:\hat{P}_{(i)}|\vec{J}^{(i)}\rangle=|\vec{J}^{(i)}\rangle} |g_i\vec{J}^{(i)}\rangle\langle e_i\vec{J}^{(i)}| + \sum_{\vec{J}^{(i)}:\hat{Q}_{(i)}|\vec{J}^{(i)}\rangle=|\vec{J}^{(i)}\rangle} e^{-i[M_g(\vec{J}^{(i)})-M_e(\vec{J}^{(i)})]\zeta t}|g_i\vec{J}^{(i)}\rangle\langle e_i\vec{J}^{(i)}| \\ &= |g_i\rangle\langle e_i| \otimes \hat{P}_{(i)} + \hat{\Delta}_i(t), \end{aligned} \quad (32)$$

with

$$\hat{\Delta}_i(t) := \sum_{\vec{J}^{(i)}:\hat{Q}_{(i)}|\vec{J}^{(i)}\rangle=|\vec{J}^{(i)}\rangle} e^{-i[M_g(\vec{J}^{(i)})-M_e(\vec{J}^{(i)})]\zeta t}|g_i\vec{J}^{(i)}\rangle\langle e_i\vec{J}^{(i)}| = \hat{Q}_{(i)}e^{\frac{i}{\hbar}\hat{H}_{\text{free}}t}|g_i\rangle\langle e_i|e^{-\frac{i}{\hbar}\hat{H}_{\text{free}}t}\hat{Q}_{(i)}, \quad (33)$$

an operator made of a sum of terms which oscillate with frequencies which are integer multiples of ζ . At the level of the operator $\hat{H}'_{\text{int}}(\ell)(t)$ this translates into the identity

$$\hat{H}'_{\text{int}}(\ell)(t) = \sum_{\chi \in X_\ell} \left(\sum_{i \in \chi} \hat{H}_{\chi,i}(\ell) \otimes \hat{P}_{(i)} + \sum_{i \in \chi} \hat{\Delta}_i(t) \right), \quad (34)$$

$$\hat{H}_{\chi,i}(\ell) := \frac{\hbar\Omega_\chi^{(\ell)}}{2} \left(e^{i\phi_\chi^{(\ell)}} |g_i\rangle\langle e_i| + \text{H.c.} \right). \quad (35)$$

Under the e - e blockade regime, $\eta_{\text{BR}} = |\zeta/\Omega_\chi^{(\ell)}| \gg 1$, the oscillatory part of $\hat{H}'_{\text{int}}(\ell)(t)$ evolves over time-scales that are much smaller than the typical time-scales determined by the first contribution. Enforcing a temporal coarse-graining over time intervals $T_{\text{c.g.}}$ such that $1/|\Omega_\chi^{(\ell)}| \gg T_{\text{c.g.}} \gg 1/|\zeta|$ this leads to

$$\hat{H}'_{\text{int}}(\ell)(t) \Big|_{\eta_{\text{BR}} \gg 1} \simeq \int_t^{t+T_{\text{c.r.}}} \frac{dt'}{T_{\text{c.r.}}} \hat{H}'_{\text{int}}(\ell)(t') = \sum_{\chi \in X_\ell} \sum_{i \in \chi} \hat{H}_{\chi,i}(\ell) \otimes \hat{P}_{(i)}. \quad (36)$$

Accordingly we can write

$$\begin{aligned} \overline{\text{exp}} \left[-\frac{i}{\hbar} \int_{\mathcal{T}_{\text{tot}}} dt' \hat{H}'_{\text{int}}(\ell)(t') \right] \Big|_{\eta_{\text{BR}} \gg 1} &\simeq \exp \left[-\frac{i}{\hbar} \sum_{\chi \in X_\ell} \sum_{i \in \chi} \hat{H}_{\chi,i}(\ell) \otimes \hat{P}_{(i)} \tau_\ell \right] = \prod_{\chi \in X_\ell} \exp \left[-\frac{i}{\hbar} \sum_{i \in \chi} \hat{H}_{\chi,i}(\ell) \otimes \hat{P}_{(i)} \tau_\ell \right] \\ &= \prod_{\chi \in X_\ell} \prod_{i \in \chi} \left[\hat{\mathbb{1}}_i \otimes \hat{Q}_{(i)} + \hat{U}_i^{(\ell)} \otimes \hat{P}_{(i)} \right], \end{aligned} \quad (37)$$

with $\hat{U}_i^{(\ell)}$ as in Eq. (23). Notice that in writing the last two identities we do not need to worry about the ordering of the various terms since they all commute. In particular the commutation of the terms associated with the different species of the subset X_ℓ is a direct consequence of the constraints (18) which prevents the possibility of driving two interacting species (i.e. AB or AC) in the same time window. Replacing this into Eq. (25) we hence obtain that for each time window \mathcal{T}_ℓ one has

$$\hat{U}^{(\ell)} \Big|_{\eta_{\text{BR}} \gg 1} \simeq e^{-\frac{i}{\hbar}\hat{H}_{\text{free}}\tau_\ell} \left(\prod_{\chi \in X_\ell} \prod_{i \in \chi} \left[\hat{\mathbb{1}}_i \otimes \hat{Q}_{(i)} + \hat{U}_i^{(\ell)} \otimes \hat{P}_{(i)} \right] \right) = e^{-\frac{i}{\hbar}\hat{H}_{\text{free}}\tau_\ell} \prod_{\chi \in X_\ell} \hat{U}_\chi^{(\ell)}. \quad (38)$$

Noticing that $e^{-\frac{i}{\hbar}\hat{H}_{\text{free}}\tau_\ell}$ commutes with (36) and hence with all the operators of the form (37) (see e.g. Eq. (32)), this finally allows us to express the global evolution operator (20) as

$$\hat{U}_{\text{tot}} \Big|_{\eta_{\text{BR}} \gg 1} \simeq e^{-\frac{i}{\hbar}\hat{H}_{\text{free}}\tau_{\text{tot}}} \prod_{\chi_\ell \in X_\ell} \dots \prod_{\chi_2 \in X_2} \prod_{\chi_1 \in X_1} \hat{U}_{\chi_\ell}^{(\ell)} \dots \hat{U}_{\chi_2}^{(2)} \hat{U}_{\chi_1}^{(1)}, \quad (39)$$

proving the thesis.

Dynamics of a ABACA qubit chain

In this section, we discuss the generalized case of driving a chain composed of *ABACA* qubits. Recall that each of the three qubit species can be controlled independently at different time intervals: specifically, $\Omega_A(t) \neq 0 \Rightarrow \Omega_B(t) = \Omega_C(t) = 0$, and $\Omega_B(t) \neq 0$ or $\Omega_C(t) \neq 0 \Rightarrow \Omega_A(t) = 0$. However, as seen in the transfer protocol shown in Fig. 2(b) of the main text, the *B*- and *C*-type qubits are driven simultaneously, allowing *B*-type qubits to function as *C*-type qubits and vice versa. Here we emphasize that the inclusion of a third species, *C*, serves only to reduce the number of physical qubits required—specifically by half, compared to a two-species architecture. Moreover, we stress that we need to separately drive the *B* and *C* qubits only when single qubit gates are performed. Referring to Fig. 2(a) of the main text, we consider *ABA* as the fundamental building block of our ladder. The *ABACA* chain is then constructed by combining two building blocks: *ABA* and *ACA*. If we drive the *B*- and *C*-type qubits with frequencies $\omega_{d,B} = \omega_B - 2\zeta$ and $\omega_{d,C} = \omega_C - 2\zeta$, respectively, we expect to enter a blockade regime where only transitions between the $|ggggg\rangle$ and $|gegeg\rangle$ states are allowed. The energy difference ΔE between these states can be explicitly calculated as:

$$\Delta E := E_{|ggggg\rangle} - E_{|gegeg\rangle} = (\omega_B - 2\zeta) + (\omega_C - 2\zeta), \quad (40)$$

confirming the result shown in Fig. 2(a) of the main text. This ΔE represents the gap between these states, effectively selecting only these transitions and thus emulating the blockade mechanism along an arbitrarily long chain.

B. General properties

A convenient way to rewrite the operators $\hat{U}_\chi^{(\ell)}$ defined in Eq. (22) is to introduce the parameters

$$\begin{cases} \theta^{(\ell)} := \Omega_\chi^{(\ell)} \tau_\ell, \\ \mathbf{n}_\perp^{(\ell)} := \left(\cos(\phi_\chi^{(\ell)}), \sin(\phi_\chi^{(\ell)}), 0 \right). \end{cases} \quad (41)$$

Recalling that the crossed elements of the χ -type qubits have twice the Rabi frequency of the regular ones, we can hence write

$$\begin{aligned} \hat{U}_\chi^{(\ell)} &= \prod_{i \in \chi_\ell^r} \left[\hat{\mathbf{1}}_i \otimes \hat{Q}_{\langle i \rangle} + \hat{\mathbb{R}}_i(\theta^{(\ell)}, \mathbf{n}_\perp^{(\ell)}) \otimes \hat{P}_{\langle i \rangle} \right] \prod_{i \in \chi_\ell^\times} \left[\hat{\mathbf{1}}_i \otimes \hat{Q}_{\langle i \rangle} + \hat{\mathbb{R}}_i(2\theta^{(\ell)}, \mathbf{n}_\perp^{(\ell)}) \otimes \hat{P}_{\langle i \rangle} \right] \\ &= \hat{W}_\chi(\theta^{(\ell)}, \mathbf{n}_\perp^{(\ell)}; 2\theta^{(\ell)}, \mathbf{n}_\perp^{(\ell)}), \end{aligned} \quad (42)$$

where defining χ^r and χ^\times as the regular (non crossed) and crossed subsets of χ -type qubits, we introduced

$$\begin{cases} \hat{W}_\chi(\theta', \mathbf{n}'; \theta'', \mathbf{n}'') := \hat{W}_{\chi^r}(\theta', \mathbf{n}') \hat{W}_{\chi^\times}(\theta'', \mathbf{n}''), \\ \hat{W}_\xi(\theta, \mathbf{n}) := \prod_{i \in \xi} \left[\hat{\mathbf{1}}_i \otimes \hat{Q}_{\langle i \rangle} + \hat{\mathbb{R}}_i(\theta, \mathbf{n}) \otimes \hat{P}_{\langle i \rangle} \right], \quad \xi \in \{\chi^r, \chi^\times\} \end{cases} \quad (43)$$

with

$$\hat{\mathbb{R}}_i(\theta, \mathbf{n}) := \exp[-i(\theta/2)\mathbf{n} \cdot \vec{\sigma}_i] = \cos(\theta/2)\hat{\mathbf{1}}_i - i \sin(\theta/2)\mathbf{n} \cdot \vec{\sigma}_i, \quad \vec{\sigma}_i := (\hat{\sigma}_i^{(x)}, \hat{\sigma}_i^{(y)}, \hat{\sigma}_i^{(z)}), \quad (44)$$

the single-qubit unitary rotation associated with the unit vector \mathbf{n} and the angle θ .

The transformations (43) obey some very useful properties:

1. The operators $\hat{W}_B(\theta'_B, \mathbf{n}'_B; \theta''_B, \mathbf{n}''_B)$ and $\hat{W}_C(\theta'_C, \mathbf{n}'_C; \theta''_C, \mathbf{n}''_C)$ always commute, i.e.

$$\hat{W}_B(\theta'_B, \mathbf{n}'_B; \theta''_B, \mathbf{n}''_B) \hat{W}_C(\theta'_C, \mathbf{n}'_C; \theta''_C, \mathbf{n}''_C) = \hat{W}_C(\theta'_C, \mathbf{n}'_C; \theta''_C, \mathbf{n}''_C) \hat{W}_B(\theta'_B, \mathbf{n}'_B; \theta''_B, \mathbf{n}''_B). \quad (45)$$

This is due to the fact that both the *B* and the *C* elements are not directly coupled by the ZZ interaction (see Fig. 1 of the main text). They only share ZZ coupling with the *A*-type qubits. On the contrary neither $\hat{W}_B(\theta'_B, \mathbf{n}'_B; \theta''_B, \mathbf{n}''_B)$ nor $\hat{W}_C(\theta'_C, \mathbf{n}'_C; \theta''_C, \mathbf{n}''_C)$ in general commute with $\hat{W}_A(\theta'_A, \mathbf{n}'_A; \theta''_A, \mathbf{n}''_A)$.

2. For fixed $\chi \in \{A, B, C\}$ setting $\theta' = 0$ ($\theta'' = 0$), the unitary evolution $\hat{W}_\chi(\theta', \mathbf{n}'; \theta'', \mathbf{n}'')$ reduces to the mapping $\hat{W}_{\chi^\times}(\theta'', \mathbf{n}'')$ ($\hat{W}_{\chi^r}(\theta', \mathbf{n}')$) that only act on the crossed (regular) elements of the χ -type qubits, i.e.

$$\hat{W}_{\chi^r}(\theta', \mathbf{n}') = \hat{W}_\chi(\theta', \mathbf{n}'; 0, \mathbf{n}'') , \quad \hat{W}_{\chi^\times}(\theta'', \mathbf{n}'') = \hat{W}_\chi(0, \mathbf{n}'; \theta'', \mathbf{n}'') , \quad (46)$$

(this is a trivial consequence of the fact that $\hat{P}_{\langle i \rangle} + \hat{Q}_{\langle i \rangle} = \hat{\mathbf{1}}_{\langle i \rangle}$ is the identity operator on the associated space).

3. For fixed $\chi \in \{A, B, C\}$, the crossed and regular contributions of $\hat{W}_\chi(\theta', \mathbf{n}'; \theta'', \mathbf{n}'')$ commute, i.e.

$$\hat{W}_{\chi^r}(\theta', \mathbf{n}') \hat{W}_{\chi^\times}(\theta'', \mathbf{n}'') = \hat{W}_{\chi^\times}(\theta'', \mathbf{n}'') \hat{W}_{\chi^r}(\theta', \mathbf{n}') . \quad (47)$$

4. For fixed $\chi \in \{A, B, C\}$ and $\xi \in \{\chi^r, \chi^\times\}$ the transformations $\hat{W}_\xi(\theta, \mathbf{n})$ form a group that obeys the same composition rules of the $SU(2)$ defined by unitary matrices $\hat{\mathbb{R}}_i(\theta, \mathbf{n})$. In particular we have that, given the angles θ_1, θ_2 and the unit vectors $\mathbf{n}_1, \mathbf{n}_2$, one has

$$\hat{W}_\xi(\theta_2, \mathbf{n}_2) \hat{W}_\xi(\theta_1, \mathbf{n}_1) = \hat{W}_\xi(\theta_3, \mathbf{n}_3) , \quad (48)$$

with the angle θ_3 and the unit vector \mathbf{n}_3 satisfying the identity $\hat{\mathbb{R}}_i(\theta_2, \mathbf{n}_2) \hat{\mathbb{R}}_i(\theta_1, \mathbf{n}_1) = \hat{\mathbb{R}}_i(\theta_3, \mathbf{n}_3)$. Furthermore the inverse of $\hat{W}_\xi(\theta, \mathbf{n})$ corresponds to $\hat{W}_\xi(-\theta, \mathbf{n}) = \hat{W}_\xi(\theta, -\mathbf{n})$, i.e.

$$\hat{W}_\xi^{-1}(\theta, \mathbf{n}) = \hat{W}_\xi^\dagger(\theta, \mathbf{n}) = \hat{W}_\xi(-\theta, \mathbf{n}) = \hat{W}_\xi(\theta, -\mathbf{n}) . \quad (49)$$

5. From the algebra of the single qubit rotations $\hat{\mathbb{R}}_i(\theta, \mathbf{n})$, it follows that for fixed $\chi \in \{A, B, C\}$ and $\xi \in \{\chi^r, \chi^\times\}$, given \mathbf{n} an arbitrary unit vector, the transformations $\hat{W}_\xi(\theta, \mathbf{n})$ are periodic in θ with period 4π , i.e.

$$\hat{W}_\xi(4\pi + \theta, \mathbf{n}) = \hat{W}_\xi(\theta, \mathbf{n}) . \quad (50)$$

In particular for $\theta = 4\pi$ the transformation coincides with the identity. Notice however that for $\theta = 2\pi$ the evolution corresponds to a non trivial phase-transformation on the ξ -type qubits,

$$\begin{cases} \hat{W}_\xi(4\pi, \mathbf{n}) = \hat{W}_\xi(0, \mathbf{n}) = \prod_{i \in \xi} \hat{\mathbf{1}}_i \otimes [\hat{Q}_{\langle i \rangle} + \hat{P}_{\langle i \rangle}] = \hat{\mathbf{1}} , \\ \hat{W}_\xi(2\pi, \mathbf{n}) = \hat{Z}_\xi^{(\text{tot})} := \prod_{i \in \xi} \hat{\mathbf{1}}_i \otimes [\hat{Q}_{\langle i \rangle} - \hat{P}_{\langle i \rangle}] = \prod_{i \in \xi} [\hat{Q}_{\langle i \rangle} - \hat{P}_{\langle i \rangle}] . \end{cases} \quad (51)$$

6. The property (48) for χ^r and χ^\times translates in the following composition rule for the global operations, i.e.

$$\hat{W}_\chi(\theta'_2, \mathbf{n}'_2; \theta''_2, \mathbf{n}''_2) \hat{W}_\chi(\theta'_1, \mathbf{n}'_1; \theta''_1, \mathbf{n}''_1) = \hat{W}_\chi(\theta'_3, \mathbf{n}'_3; \theta''_3, \mathbf{n}''_3) , \quad (52)$$

with θ'_3, \mathbf{n}'_3 , and $\theta''_3, \mathbf{n}''_3$ determined by the identities $\hat{\mathbb{R}}_i(\theta'_2, \mathbf{n}'_2) \hat{\mathbb{R}}_i(\theta'_1, \mathbf{n}'_1) = \hat{\mathbb{R}}_i(\theta'_3, \mathbf{n}'_3)$ and $\hat{\mathbb{R}}_i(\theta''_2, \mathbf{n}''_2) \hat{\mathbb{R}}_i(\theta''_1, \mathbf{n}''_1) = \hat{\mathbb{R}}_i(\theta''_3, \mathbf{n}''_3)$, respectively.

C. Universal control

In Sec. II A we have seen that in the e - e blockade regime, each individual pulsed unitary $\hat{U}^{(\ell)}$ that compose \hat{U}_{tot} implements a specific type of control unitary gates (43), i.e. the subset of transformations

$$\hat{W}_\chi(\theta, \mathbf{n}_\perp; 2\theta, \mathbf{n}_\perp) = \hat{W}_{\chi^r}(\theta, \mathbf{n}_\perp) \hat{W}_{\chi^\times}(2\theta, \mathbf{n}_\perp) , \quad (53)$$

which act simultaneously on χ^r and χ^\times inducing single-qubit rotations around a generic unit vector \mathbf{n}_\perp of the xy -plane (i.e. $\mathbf{z} \cdot \mathbf{n}_\perp = 0$) and with correlated angles θ and 2θ . Here we show that these constraints can be overcome by properly combining sequences of these special type of pulses: specifically we prove that the sequences (20) generated by the classical controls of the ladder, can produce any transformation $\hat{W}_\chi(\theta', \mathbf{n}'; \theta'' \mathbf{n}'')$ with θ', θ'' , and $\mathbf{n}', \mathbf{n}''$ arbitrarily selected. The first ingredient to attain this result is a property that holds for Pauli rotations along orthogonal unit vectors, i.e.

$$\mathbf{n} \cdot \mathbf{m} = 0 \quad \implies \quad \hat{\mathbb{R}}_i(\pi, -\mathbf{n}) \hat{\mathbb{R}}_i(\theta, \mathbf{m}) \hat{\mathbb{R}}_i(\pi, \mathbf{n}) = \hat{\mathbb{R}}_i(-\theta, \mathbf{m}) = \hat{\mathbb{R}}_i^{-1}(\theta, \mathbf{m}) \quad \forall \theta . \quad (54)$$

This identity is a direct consequence of the fact that $\hat{\mathbb{R}}_i(\pi, \mathbf{n}) = -i\mathbf{n} \cdot \vec{\sigma}_i$, and that the Pauli operators $(\mathbf{n} \cdot \vec{\sigma}_i)$ and $(\mathbf{m} \cdot \vec{\sigma}_i)$ anti-commute, i.e. $(\mathbf{n} \cdot \vec{\sigma}_i)(\mathbf{m} \cdot \vec{\sigma}_i)(\mathbf{n} \cdot \vec{\sigma}_i) = -\mathbf{m} \cdot \vec{\sigma}_i$. Recalling that $\hat{\mathbb{R}}_i(2\pi, \mathbf{n}) = -\hat{\mathbb{1}}_i$, we can hence conclude that

$$\begin{cases} \hat{\mathbb{R}}_i(\pi, -\mathbf{n})\hat{\mathbb{R}}_i(\theta, \mathbf{m})\hat{\mathbb{R}}_i(\pi, \mathbf{n})\hat{\mathbb{R}}_i(\theta, \mathbf{m}) = \hat{\mathbb{R}}_i(0, \mathbf{m}) = \hat{\mathbb{1}}_i, \\ \hat{\mathbb{R}}_i(2\pi, -\mathbf{n})\hat{\mathbb{R}}_i(2\theta, \mathbf{m})\hat{\mathbb{R}}_i(2\pi, \mathbf{n})\hat{\mathbb{R}}_i(2\theta, \mathbf{m}) = \hat{\mathbb{R}}_i(4\theta, \mathbf{m}). \end{cases} \quad (55)$$

Consider hence a 4-pulse sequence (20), $\hat{U}_\chi^{(4)}\hat{U}_\chi^{(3)}\hat{U}_\chi^{(2)}\hat{U}_\chi^{(1)}$, where the first and the third element, $\hat{U}_\chi^{(1)}$ and $\hat{U}_\chi^{(3)}$, correspond to the same transformation $\hat{W}_\chi(\theta/4, \mathbf{n}_\perp; \theta/2, \mathbf{n}_\perp)$ (see Eq. (42)) with assigned axis \mathbf{n}_\perp in the xy -plane. On the contrary the second and fourth term, $\hat{U}_\chi^{(2)}$ and $\hat{U}_\chi^{(4)}$, are equal to $\hat{W}_\chi(\pi, \mathbf{m}_\perp; 2\pi, \mathbf{m}_\perp)$ and $\hat{W}_\chi(\pi, -\mathbf{m}_\perp; 2\pi, -\mathbf{m}_\perp)$, respectively with \mathbf{m}_\perp also in the xy -plane but orthogonal to \mathbf{n}_\perp (i.e. $\mathbf{m}_\perp \cdot \mathbf{n}_\perp = 0$). Using Eq. (39), the composition rule given in Eq. (52) and the identities (55) we can hence conclude that

$$\begin{aligned} \hat{U}_\chi^{(4)}\hat{U}_\chi^{(3)}\hat{U}_\chi^{(2)}\hat{U}_\chi^{(1)} \Big|_{\eta_{\text{BR}} \gg 1} &\simeq \hat{W}_\chi(\pi, -\mathbf{m}_\perp; 2\pi, -\mathbf{m}_\perp)\hat{W}_\chi(\theta/4, \mathbf{n}_\perp; \theta/2, \mathbf{n}_\perp)\hat{W}_\chi(\pi, \mathbf{m}_\perp; 2\pi, \mathbf{m}_\perp)\hat{W}_\chi(\theta/4, \mathbf{n}_\perp; \theta/2, \mathbf{n}_\perp) \\ &= \hat{W}_\chi(0, \mathbf{n}_\perp; \theta, \mathbf{n}_\perp) = \hat{W}_{\chi^\times}(\theta, \mathbf{n}_\perp), \end{aligned} \quad (56)$$

which for sake of simplicity we write dropping the contribution $\exp\left[-\frac{i}{\hbar}\hat{H}_{\text{free}}\tau_{\text{tot}}\right]$. Equation (56) implies that using the control pulses of the model we can generate transformations that act selectively on the crossed elements of the χ -type qubits inducing arbitrary rotations around any axis \mathbf{n}_\perp in the xy -plane (in particular we can induce rotations around the \mathbf{x} and \mathbf{y} axis). Invoking the standard Euler rotation theorem [S11] we can generalize this to any control-unitary $\hat{W}_{\chi^\times}(\theta, \mathbf{n})$ with respect to any possible (non necessarily orthogonal to \mathbf{z}) axis \mathbf{n} . Indeed recall that given (θ, \mathbf{n}) arbitrary, there exist three angles α , β , and γ , such that we can write

$$\hat{\mathbb{R}}_i(\alpha, \mathbf{x})\hat{\mathbb{R}}_i(\beta, \mathbf{y})\hat{\mathbb{R}}_i(\gamma, \mathbf{x}) = \hat{\mathbb{R}}_i(\theta, \mathbf{n}). \quad (57)$$

Using sequences of the form (56) we can hence translate the above identity at the level of our control unitary gates, obtaining

$$\hat{W}_{\chi^\times}(\alpha, \mathbf{x})\hat{W}_{\chi^\times}(\beta, \mathbf{y})\hat{W}_{\chi^\times}(\gamma, \mathbf{x}) = \hat{W}_{\chi^\times}(\theta, \mathbf{n}). \quad (58)$$

Notice that to achieve this goal one needs no more than $3 \times 4 = 12$ unitary pulses \hat{U}_χ . A similar result can be applied to the control unitaries that act selectively on the regular elements of the χ -type qubits. For instance using the transformation (56) we can compensate the χ^\times component of the gates (53), i.e.

$$\hat{W}_{\chi^\times}(2\theta, -\mathbf{n}_\perp)\hat{W}_\chi(\theta, \mathbf{n}_\perp; 2\theta, \mathbf{n}_\perp) = \hat{W}_{\chi^r}(\theta, \mathbf{n}_\perp), \quad (59)$$

which shows that also for the regular elements of the χ -type qubits we can induce arbitrary rotation around any axis \mathbf{n}_\perp in the xy -plane. From this we can then use the argument that led us to (58) to conclude that sequences unitary pulses \hat{U}_χ can leads to any operations of the form $\hat{W}_{\chi^r}(\theta, \mathbf{n})$ with arbitrary \mathbf{n} and θ , i.e.

$$\hat{W}_{\chi^r}(\alpha, \mathbf{x})\hat{W}_{\chi^r}(\beta, \mathbf{y})\hat{W}_{\chi^r}(\gamma, \mathbf{x}) = \hat{W}_{\chi^r}(\theta, \mathbf{n}). \quad (60)$$

Finally concatenating the results of Eqs. (58) and (60) we can induce any arbitrary transformations of the form $\hat{W}_\chi(\theta', \mathbf{n}'; \theta'', \mathbf{n}'')$.

III. INFORMATION ENCODING AND QUANTUM COMPUTING

As discussed in the main text, our model encodes the information in one of the columns of the device. Specifically at each step of the computation, we assume the ladder to be in a state of the form

$$|\Psi; k\rangle := \left(\cdots |g^{\otimes N}\rangle_{k-3} \otimes |e^{\otimes N}\rangle_{k-2} \otimes |g^{\otimes N}\rangle_{k-1} \right) \otimes |\Psi\rangle_k \otimes \left(|g^{\otimes N}\rangle_{k+1} \otimes |g^{\otimes N}\rangle_{k+2} \otimes |g^{\otimes N}\rangle_{k+3} \cdots \right) \otimes |g^{\otimes(N-1)}\rangle_{A^\times}. \quad (61)$$

In this expression the ket $|\cdots\rangle_{k'}$ describes the state of the k' -th column of the device: in particular $|g^{\otimes N}\rangle_{k'}$ ($|e^{\otimes N}\rangle_{k'}$) represents the case where all the qubits of the k' -th column are in the $|g\rangle$ ($|e\rangle$) configuration. $|\Psi\rangle_k$ is the logical (possibly entangled) state of the ICC, and $|g^{\otimes(N-1)}\rangle_{A^\times}$ describes the state of the $N - 1$ crossed A -type qubits which

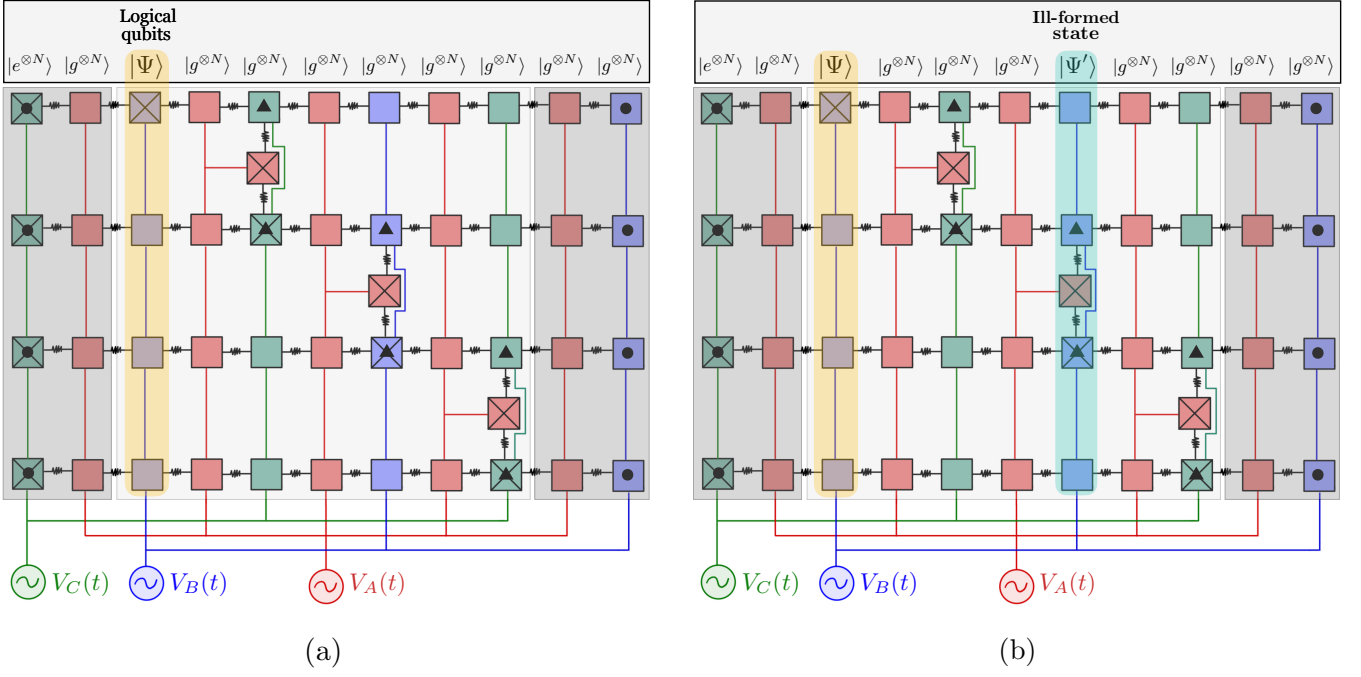


FIG. 2: Panel (a): example of a B -type well-formed state (61) which we use to encode the logical information in the device that allows the computation with $N = 4$ logical qubits. The yellow area identifies the Information Carrying Column (ICC): the columns on the left of the ICC are in a paramagnetic phase, while the columns on the right are in a ferromagnetic phase. The crossed red elements that act as couplers for the various rows of the ladder are also in ferromagnetic ($|gg..g\rangle$) phase. Panel (b): example of a well-behaved, ill-formed state $|\tilde{\Psi}; k\rangle$ obtained by deteriorating the state of panel (a) by replacing one of the B columns on the right-hand-side with a non-ferromagnetic term: under $\hat{Z}_{A^r}^{\text{tot}}$ this state transforms as in Eq. (74).

act as connectors between adjacent rows (notice that in writing Eq. (7) of the main text the presence of the last contribution was dropped for ease of notation). It is also worth stressing that, in our model, these are the only crossed elements of A -type; in particular, all the A columns of the ladder are composed of only regular (non-crossed) elements.

States as defined in Eq. (61) are said to be *well-formed* (see panel (a) of Fig. 2 for an example). These states exhibit no quantum correlations among the different qubits of the device, except for those located in the ICC, which are the only ones that can share entanglement. An alternative, more compact way to express them is:

$$|\Psi; k\rangle = |\text{para}\rangle \otimes |\Psi\rangle_k \otimes |\text{ferro}\rangle, \quad (62)$$

which emphasises that the ICC is an interface between a paramagnetic region on the left, where, starting from the rightmost element which is always in $|g^{\otimes N}\rangle$, all the columns are prepared in an alternating sequence of $|g^{\otimes N}\rangle$ and $|e^{\otimes N}\rangle$ configurations, and a ferromagnetic region on the right where all the columns are instead in the $|g^{\otimes N}\rangle$ configuration. In this compact notation, the ferromagnetic region always includes also the crossed qubits of type A . The procedure for initializing the ladder in this special type of states will be discussed in Sec. III E. Here, instead, we discuss how the well-formed state of the model evolves under the action of the system Hamiltonian.

Remark: To simplify the presentation in the following Section, we shall introduce the special notation “ $\stackrel{*}{\equiv}$ ” to indicate that two vector states of the system are equal up to an (irrelevant, not state dependent) global phase. Specifically:

$$|a\rangle \stackrel{*}{\equiv} |b\rangle \quad \implies \quad \exists e^{i\varphi} \text{ s.t. } |a\rangle = e^{i\varphi} |b\rangle. \quad (63)$$

A. Preliminary observations

To begin with, let us note a few useful properties.

i) In our analysis we will only use states $|\Psi; k\rangle$ with values of k that are larger than or equal to 3 (i.e., the first column of the processing area of the device). In other words, the logical information will always be located either in the processing area or in the read-out area, never in the initialization area. Additionally, the $|\Psi; k\rangle$'s can be categorized into three groups:

- **A-type well-formed states:** these are states $|\Psi; k\rangle$ where the ICC index k identifies a column of the ladder formed by A -type qubits;
- **B-type well-formed states:** these are states $|\Psi; k\rangle$ where the ICC index k identifies a column of the ladder formed by B -type qubits;
- **C-type well-formed states:** these are states $|\Psi; k\rangle$ where the ICC index k identifies a column of the ladder formed by C -type qubits.

ii) The well-formed states $|\Psi; k\rangle$ are invariant under the action of the global unitary $e^{-\frac{i}{\hbar}\hat{H}_{\text{free}}\tau_{\text{tot}}}$ which enters in the decomposition (20). Specifically,

$$e^{-\frac{i}{\hbar}\hat{H}_{\text{free}}\tau_{\text{tot}}}|\Psi; k\rangle = e^{-2i\zeta\tau_{\text{tot}}\sum_{\langle i,j\rangle}|e_i e_j\rangle\langle e_i e_j|}|\Psi; k\rangle = |\Psi; k\rangle. \quad (64)$$

This is due to the special arrangement of the interactions in the ladder, where in the state $|\Psi; k\rangle$, each ZZ-interacting pair $\langle i, j\rangle$ has at least one element that is in the ground state, so $\langle e_i e_j|\Psi; k\rangle = 0$. Thanks to Eq. (64), and recalling that $e^{-\frac{i}{\hbar}\hat{H}_{\text{free}}\tau_{\text{tot}}}$ commutes with all the $\hat{U}_\chi^{(\ell)}$ terms, we can write

$$\hat{U}_{\text{tot}}\Big|_{\eta_{\text{BR}}\gg 1}|\Psi; k\rangle \simeq \hat{U}_\chi^{(\ell)}\dots\hat{U}_\chi^{(2)}\hat{U}_\chi^{(1)}|\Psi; k\rangle, \quad (65)$$

which justifies dropping $e^{-\frac{i}{\hbar}\hat{H}_{\text{free}}\tau_{\text{tot}}}$ in Eq. (56) and in Eq. (5) of the main text.

iii) Let $|\Psi; k\rangle$ be a B - or C -type well-formed state. The application of the gate $\hat{Z}_{A_r}^{\text{tot}}$ of Eq. (51) induces the following mapping:

$$\hat{Z}_{A_r}^{\text{tot}}|\Psi; k\rangle \stackrel{*}{=} \left|[\hat{\sigma}^{(z)}]^{\otimes N}\Psi; k\right\rangle := |\text{para}\rangle \otimes [\hat{\sigma}^{(z)}]^{\otimes N}|\Psi\rangle_k \otimes |\text{ferro}\rangle, \quad (66)$$

where $|\left[\hat{\sigma}^{(z)}\right]^{\otimes N}\Psi; k\rangle$ represents a well-formed state of the system with the ICC still located in the k -th column of the device, but with the internal state of the logical qubits evolved under the action of a contemporary application of $\hat{\sigma}^{(z)}$ gates. To see why Eq. (66) holds, recall that $\hat{Z}_{A_r}^{\text{tot}}$ acts selectively on the regular A -type qubits of the model, applying to each of them a control- 2π rotation, i.e. a control-phase shift of -1 . Observe that, since the ICC column is of B - or C -type, then the only A -type columns that can acquire such extra phase, are those in the ferromagnetic area. Indeed all the A -type columns on the left-hand-side of the ICC have at least either an interacting neighbouring B or C element that is in the excited state. Apart from the first one, the A -type columns in the ferromagnetic region are coupled with neighbouring B - and C -type qubits which are in a definite ground state $|g\rangle$ – see panel (a) of Fig. 2. Acting on them, $\hat{Z}_{A_r}^{\text{tot}}$ will assign to the state an irrelevant global phase that is a product of (-1) 's. The exact number M_k of such terms depends on the actual location of ICC column. For instance in the case shown in the panel (a) of Fig. 2, the global phase induced by $\hat{Z}_{A_r}^{\text{tot}}$ is $(-1)^{\dots} = \dots$. In the end the only non trivial effect that $\hat{Z}_{A_r}^{\text{tot}}$ can introduce in the model occurs when it acts on the first A -type column of the ferromagnetic area. For future reference we shall identify such column with the symbol \mathcal{A}_*^r . Due to the presence of the ICC, the activation of the (-1) phase on the j -th row element of this column depends on the state of the j -th logical qubit (observe that the only other B - or C -type column that is ZZ coupled with \mathcal{A}_*^r has all the qubits in the $|g\rangle$ state). To formalize this, define $\hat{Z}_{\mathcal{A}_*^r}^{\text{tot}}$ as the restriction of $\hat{Z}_{A_r}^{\text{tot}}$ on the column \mathcal{A}_*^r , i.e.

$$\hat{Z}_{\mathcal{A}_*^r}^{\text{tot}} := \prod_{i \in \mathcal{A}_*^r} \left[\hat{Q}_{\langle i\rangle} - \hat{P}_{\langle i\rangle} \right]. \quad (67)$$

From the previous analysis, we can write:

$$\hat{Z}_{A_r}^{\text{tot}}|\Psi; k\rangle = (-1)^{M_k}\hat{Z}_{\mathcal{A}_*^r}^{\text{tot}}|\Psi; k\rangle = (-1)^{M_k}\prod_{i \in \mathcal{A}_*^r} \left[\hat{Q}_{\langle i\rangle} - \hat{P}_{\langle i\rangle} \right]|\Psi; k\rangle. \quad (68)$$

Notice that $\hat{Q}_{(i)} - \hat{P}_{(i)}$ is a control-phase gate that act on the i -th qubit of \mathcal{A}_*^r , which is activated if and only if its two ZZ coupled neighbouring qubits are both in the ground state. To make use of this fact expand the logical state $|\Psi\rangle$ of the ICC as

$$|\Psi\rangle = |g_i\Psi_g\rangle + |e_i\Psi_e\rangle \quad \Longrightarrow \quad |\Psi; k\rangle = |g_i\Psi_g; k\rangle + |e_i\Psi_e; k\rangle, \quad (69)$$

where $|g_i\rangle$ and $|e_i\rangle$ are the ground and excited state of the element pertaining to the ICC column that is on the same row of i -th qubit of \mathcal{A}_*^r , $|\Psi_g\rangle$ and $|\Psi_e\rangle$ are (non necessarily normalized) states of the remaining $N - 1$ elements of the ICC column. Observe then that

$$\begin{cases} \hat{Q}_{(i)}|\Psi; k\rangle = |e_i\Psi_e; k\rangle, \\ \hat{P}_{(i)}|\Psi; k\rangle = |g_i\Psi_g; k\rangle, \end{cases} \quad \Longrightarrow \quad (\hat{Q}_{(i)} - \hat{P}_{(i)})|\Psi; k\rangle = -|g_i\Psi_g; k\rangle + |e_i\Psi_e; k\rangle = \hat{\sigma}_i^{(z)}|\Psi; k\rangle, \quad (70)$$

which when replaced in the previous Eq. (68) gives

$$\hat{Z}_{A^r}^{\text{tot}}|\Psi; k\rangle = (-1)^{M_k} \prod_{i \in \mathcal{A}_*^r} \hat{\sigma}_i^{(z)}|\Psi; k\rangle = (-1)^{M_k} \left| [\hat{\sigma}^{(z)}]^{\otimes N} \Psi; k \right\rangle, \quad (71)$$

proving Eq. (66).

- iv) The property (66) also holds for certain ill-formed states of the ladder. In particular this occurs if one or more of the B -type (C -type) columns in the ferromagnetic phase of a B -type (C -type) well-formed state $|\Psi; k\rangle$ are replaced by arbitrary qubit states (see panel (b) of Fig. 2 for an example of a configuration that meets these requirements). An ill-formed state of this type will be said to be *well-behaved*. Under these conditions, each of the two A columns near a deteriorated B column of well-behaved, ill-formed B -type state has an extra C column that is still initialized in the proper ferromagnetic configuration $|g^{\otimes N}\rangle$. Thus, when $\hat{Z}_{A^r}^{\text{tot}}$ is applied to the system, a deteriorated B column will act as the unique controller for its two neighbouring A elements, assigning the same conditional (-1) phase to both, ultimately not modifying the state. A similar effect will occur in case of well-behaved, ill-formed C -type state: here each of the two A columns near a deteriorated C column will have an extra B column that is still initialized in the proper ferromagnetic configuration $|g^{\otimes N}\rangle$.

To see this explicitly let us consider in details the case of a well-behaved, ill-formed B -type state. $|\tilde{\Psi}; k\rangle$ (the analysis of the well-behaved, ill-formed C -type states will follows along the same path). Define $\{\tilde{\mathcal{B}}_1, \tilde{\mathcal{B}}_2, \dots, \tilde{\mathcal{B}}_S\}$ the set of its deformed columns. Let $\tilde{\mathcal{A}}_\ell^{(\text{left})}$ and $\tilde{\mathcal{A}}_\ell^{(\text{right})}$ the A columns on the left-hand side and right-hand side, respectively, of the ℓ -th element of this set. As in the case of Eq. (71) we can write

$$\hat{Z}_{A^r}^{\text{tot}}|\tilde{\Psi}; k\rangle = (-1)^{M'_k} \hat{Z}_{\mathcal{A}_*^r}^{\text{tot}} \prod_{\ell=1}^S \hat{Z}_{\tilde{\mathcal{A}}_\ell^{(\text{left})}}^{\text{tot}} \hat{Z}_{\tilde{\mathcal{A}}_\ell^{(\text{right})}}^{\text{tot}} |\tilde{\Psi}; k\rangle, \quad (72)$$

where the global phase $(-1)^{M'_k}$ depends on the number M'_k of ferromagnetic B columns that are not deteriorated. Here $\hat{Z}_{\mathcal{A}}^{\text{tot}} := \prod_{i \in \mathcal{A}} [\hat{Q}_{(i)} - \hat{P}_{(i)}]$ indicates the part of $\hat{Z}_{A^r}^{\text{tot}}$ that involves elements of the \mathcal{A} column. Due to the commutativity of the operators $[\hat{\mathbb{1}}_i \otimes \hat{Q}_{(i)} + \hat{\mathbb{R}}_i(\theta, \mathbf{n}) \otimes \hat{P}_{(i)}]$ associated with different qubits, $\hat{Z}_{\mathcal{A}}^{\text{tot}}$ of different columns commute. Following the same derivation used in Eq. (71), we then can show that

$$\hat{Z}_{\tilde{\mathcal{A}}_\ell^{(\text{left})}}^{\text{tot}} \hat{Z}_{\tilde{\mathcal{A}}_\ell^{(\text{right})}}^{\text{tot}} |\tilde{\Psi}; k\rangle = \hat{Z}_{\tilde{\mathcal{A}}_\ell^{(\text{left})}}^{\text{tot}} \left(\prod_{i \in \tilde{\mathcal{B}}_\ell} \hat{\sigma}_i^{(z)} |\tilde{\Psi}; k\rangle \right) = \prod_{i' \in \tilde{\mathcal{B}}_\ell} \hat{\sigma}_{i'}^{(z)} \prod_{i \in \tilde{\mathcal{B}}_\ell} \hat{\sigma}_i^{(z)} |\tilde{\Psi}; k\rangle = |\tilde{\Psi}; k\rangle, \quad (73)$$

so that

$$\hat{Z}_{A^r}^{\text{tot}}|\tilde{\Psi}; k\rangle = (-1)^{M'_k} \hat{Z}_{\mathcal{A}_*^r}^{\text{tot}}|\tilde{\Psi}; k\rangle = (-1)^{M'_k} \left| [\hat{\sigma}^{(z)}]^{\otimes N} \tilde{\Psi}; k \right\rangle, \quad (74)$$

which proves the thesis.

B. Motion of the interface

As we have mentioned in the main text, by applying a specific sequence of pulses (39) we can generate a unitary transformation \hat{U}_{shift} that rigidly moves the interface from left to right, i.e.

$$\hat{U}_{\text{shift}}|\Psi; k\rangle \stackrel{*}{=} |\Psi; k + 1\rangle, \quad (75)$$

for all $3 \leq k \leq 2N$ (recall that the total numbers of column in the model is $2N + 3$). In particular given

$$\hat{\Pi}_\xi := \hat{W}_\xi(\pi; \mathbf{x}) = \prod_{i \in \xi} \left[\hat{\mathbf{1}}_i \otimes \hat{Q}_{\langle i \rangle} - i\hat{\sigma}_i^{(x)} \otimes \hat{P}_{\langle i \rangle} \right], \quad (76)$$

this can be done e.g. by taking

$$\hat{U}_{\text{shift}} = \begin{cases} \hat{\Pi}_{A^r} \hat{\Pi}_B \hat{\Pi}_C \hat{\Pi}_{A^r} & \text{if } |\Psi; k\rangle \text{ is either a } B \text{ or } C\text{-type well-formed state;} \\ \hat{\Pi}_B \hat{\Pi}_C \hat{\Pi}_{A^r} \hat{\Pi}_B \hat{\Pi}_C & \text{if } |\Psi; k\rangle \text{ is a } A\text{-type well-formed state,} \end{cases} \quad (77)$$

which we write omitting the term $e^{-\frac{i}{\hbar} \hat{H}_{\text{free}} \tau_{\text{tot}}}$ due to property ii) of Sec. III A. To verify that our choice of \hat{U}_{shift} is correct, consider the case where $|\Psi; k\rangle$ is a B -type well-formed state (the analysis for the other cases is similar and will not be reported here). To study the evolution of this state under the sequence $\hat{\Pi}_{A^r} \hat{\Pi}_B \hat{\Pi}_C \hat{\Pi}_{A^r}$ it is worth splitting the vector $|\Psi; k\rangle$ in the following four sectors:

$$|\Psi; k\rangle := \underbrace{\left(\cdots |g_A^{\otimes N}\rangle_{k-5} \otimes |e_B^{\otimes N}\rangle_{k-4} \otimes |g_A^{\otimes N}\rangle_{k-3} \otimes |e_C^{\otimes N}\rangle_{k-2} \otimes |g_A^{\otimes N}\rangle_{k-1} \right)}_{\text{sector I}} \otimes \underbrace{\left(|\Psi_B\rangle_k \otimes |g_A^{\otimes N}\rangle_{k+1} \right)}_{\text{sector II}} \\ \otimes \underbrace{\left(|g_C^{\otimes N}\rangle_{k+2} \otimes |g_A^{\otimes N}\rangle_{k+3} \otimes |g_B^{\otimes N}\rangle_{k+4} \otimes |g_A^{\otimes N}\rangle_{k+5} \cdots \right)}_{\text{sector III}} \otimes \underbrace{|g^{\otimes(N-1)}\rangle_{A^\times}}_{\text{sector IV}} \quad (78)$$

where we add the subscripts A , B , and C to the various terms to specify the type of the column.

- **Sector IV:** First of all, it is clear that since the crossed A -type qubits are not affected by the selected controls, the term in sector IV will be left unchanged by the evolution, i.e.

$$|g^{\otimes(N-1)}\rangle_{A^\times} \xrightarrow{\hat{\Pi}_{A^r} \hat{\Pi}_B \hat{\Pi}_C \hat{\Pi}_{A^r}} |g^{\otimes(N-1)}\rangle_{A^\times}. \quad (79)$$

Most importantly, it is worth stressing that the crossed A elements will remain in the $|g\rangle$ state at *all times* during the entire pulse sequence. This fact is extremely important as it means that these qubits play no role what-so-ever in the evolution of the other qubits of the device. In particular the possibility that a given control-pulse will be activated on one of the qubits that are ZZ coupled with a crossed A -type element, does not depend on the latter since it will be always in the “go” state.

- **Sector I:** According to Eq. (78) the qubits of this sector are initialized in the paramagnetic phase. As evident from the equation in this case the A columns have at least a nearby B or C column in the $|e^{\otimes N}\rangle$ which prevents the first $\hat{\Pi}_{A^r}$ of the sequence to operate on them. Viceversa, when we apply $\hat{\Pi}_B$, since all the B columns have neighbouring A -type qubits which are all in $|g\rangle$, they will experience $-i\hat{\sigma}_i^{(x)}$ rotations that will map them into $(-i)^N |g^{\otimes N}\rangle$. The final $\hat{\Pi}_{A^r}$ operation will hence not be blocked, modifying the states of the A -type qubits in the paramagnetic area via $-i\hat{\sigma}_i^{(x)}$ pulses. The same happens to the C columns when we operate with $\hat{\Pi}_C$ (recall that due to the commutative property Eq. (45) the order in which we apply $\hat{\Pi}_B$ and $\hat{\Pi}_C$ does not matter). The global trajectory induced by the unitary \hat{U}_{shift} on the component (80) of $|\Psi; k\rangle$ can hence be expressed as

$$\begin{aligned} \cdots |e_B^{\otimes N}\rangle_{k-4} \otimes |g_A^{\otimes N}\rangle_{k-3} \otimes |e_C^{\otimes N}\rangle_{k-2} \otimes |g_A^{\otimes N}\rangle_{k-1} &\xrightarrow{\hat{\Pi}_{A^r}} \cdots |e_B^{\otimes N}\rangle_{k-4} \otimes |g_A^{\otimes N}\rangle_{k-3} \otimes |e_C^{\otimes N}\rangle_{k-2} \otimes |g_A^{\otimes N}\rangle_{k-1} \\ &\xrightarrow{\hat{\Pi}_B} \cdots |g_B^{\otimes N}\rangle_{k-4} \otimes |g_A^{\otimes N}\rangle_{k-3} \otimes |e_C^{\otimes N}\rangle_{k-2} \otimes |g_A^{\otimes N}\rangle_{k-1} \\ &\xrightarrow{\hat{\Pi}_C} \cdots |g_B^{\otimes N}\rangle_{k-4} \otimes |g_A^{\otimes N}\rangle_{k-3} \otimes |g_C^{\otimes N}\rangle_{k-2} \otimes |g_A^{\otimes N}\rangle_{k-1} \\ &\xrightarrow{\hat{\Pi}_{A^r}} \cdots |g_B^{\otimes N}\rangle_{k-4} \otimes |e_A^{\otimes N}\rangle_{k-3} \otimes |g_C^{\otimes N}\rangle_{k-2} \otimes |e_A^{\otimes N}\rangle_{k-1}, \end{aligned} \quad (80)$$

up to an irrelevant global phase shift given by $(-i)^{M_k}$ with M_k counting the total number of the applied $-i\hat{\sigma}_i^{(x)}$ rotations (a number that depends only on k).

- **Sector III:** In this case it is clear that the first $\hat{\Pi}_{A^r}$ can induce $-i\hat{\sigma}_i^{(x)}$ rotation on all the A columns, bringing them into $|e^{\otimes N}\rangle$ states which, in turn, will prevent the action of $\hat{\Pi}_B$ and $\hat{\Pi}_C$. The final operator $\hat{\Pi}_{A^r}$ will still be able to act returning all the A column to their original configuration, i.e.

$$\begin{aligned}
|g_C^{\otimes N}\rangle_{k+2} \otimes |g_A^{\otimes N}\rangle_{k+3} \otimes |g_B^{\otimes N}\rangle_{k+4} \otimes |g_A^{\otimes N}\rangle_{k+5} \cdots &\xrightarrow{\hat{\Pi}_{A^r}} |g_C^{\otimes N}\rangle_{k+2} \otimes |e_A^{\otimes N}\rangle_{k+3} \otimes |g_B^{\otimes N}\rangle_{k+4} \otimes |e_A^{\otimes N}\rangle_{k+5} \cdots \\
&\xrightarrow{\hat{\Pi}_B} |g_C^{\otimes N}\rangle_{k+2} \otimes |e_A^{\otimes N}\rangle_{k+3} \otimes |g_B^{\otimes N}\rangle_{k+4} \otimes |e_A^{\otimes N}\rangle_{k+5} \cdots \\
&\xrightarrow{\hat{\Pi}_C} |g_C^{\otimes N}\rangle_{k+2} \otimes |e_A^{\otimes N}\rangle_{k+3} \otimes |g_B^{\otimes N}\rangle_{k+4} \otimes |e_A^{\otimes N}\rangle_{k+5} \cdots \\
&\xrightarrow{\hat{\Pi}_{A^r}} |g_C^{\otimes N}\rangle_{k+2} \otimes |g_A^{\otimes N}\rangle_{k+3} \otimes |g_B^{\otimes N}\rangle_{k+4} \otimes |g_A^{\otimes N}\rangle_{k+5} \cdots .
\end{aligned} \tag{81}$$

- **Sector II:** The study of this sector is slightly more complex since in this case the various pulses induce correlations among involved columns (i.e. the ICC column and its first neighbour on the right). To begin with it is clear that $\hat{\Pi}_C$ will not have effects on the sector as it does not include C qubits. A useful observation is also that when we apply the two $\hat{\Pi}_{A^r}$ transformations of the sequence, the action of these operators on the $(k+1)$ -th column (which is of A -type), only depends on the internal state of the ICC column, due to the fact that the C column at position $k+2$ is in the state $|g^{\otimes N}\rangle$ – see Eq. (81). Similarly when we apply the $\hat{\Pi}_B$, its action on the ICC column only depends on the $(k+1)$ -th column, due to the fact that the A column at position $k-1$ is in $|g^{\otimes N}\rangle$ as shown in Eq. (80) (recall that the crossed A -type qubits are always in the $|g\rangle$ during the entire process). We can hence conclude that, despite our control pulses affect more than two qubits at the time, thanks to the selected encoding, the net effect of the sequence $\hat{\Pi}_{A^r}\hat{\Pi}_B\hat{\Pi}_{A^r}$ is to effectively induce a selective coupling between column k with column $k+1$. To study explicitly what type of evolution this induces in our model, it is useful to consider first the scenario where the ladder is formed by a single row. In this case the state of sector II can be explicitly expressed as

$$|\Psi_B\rangle_k \otimes |g_A\rangle_{k+1} = \alpha|g_B\rangle_k \otimes |g_A\rangle_{k+1} + \beta|e_B\rangle_k \otimes |g_A\rangle_{k+1} , \tag{82}$$

where we expanded $|\Psi_B\rangle_k$ in the computational basis. We can now easily track the evolution of this configuration recalling that the various control-operations are activated either by the internal state of k -th column (in the case of $\hat{\Pi}_{A^r}$), or by the internal state of the $(k+1)$ -th column (in the case of $\hat{\Pi}_B$). Accordingly we get:

$$\begin{aligned}
|\Psi_B\rangle_k \otimes |g_A\rangle_{k+1} &\xrightarrow{\hat{\Pi}_A} -i\alpha|g_B\rangle_k \otimes |e_A\rangle_{k+1} + \beta|e_B\rangle_k \otimes |g_A\rangle_{k+1} \\
&\xrightarrow{\hat{\Pi}_B} -i\alpha|g_B\rangle_k \otimes |e_A\rangle_{k+1} - i\beta|g_B\rangle_k \otimes |g_A\rangle_{k+1} = -i|g_B\rangle_k \otimes (\alpha|e_A\rangle_{k+1} + \beta|g_A\rangle_{k+1}) \\
&\xrightarrow{\hat{\Pi}_A} (-i)^2|g_B\rangle_k \otimes (\alpha|g_A\rangle_{k+1} + \beta|e_A\rangle_{k+1}) = -|g_B\rangle_k \otimes |\Psi_A\rangle_{k+1} ,
\end{aligned} \tag{83}$$

which shows that at the end of the sequence the states of the k and $k+1$ have swapped (up to an irrelevant global phase). To generalize this result to the case of N rows, simply recall that in our model, apart from the presence of the crossed A -type qubits which in the present case are always in the $|g\rangle$ state, there are not direct interactions among the various elements of a column. This in particular implies that the dynamics induced by $\hat{\Pi}_{A^r}\hat{\Pi}_B\hat{\Pi}_{A^r}$ can be addressed treating the various rows independently. Accordingly we can conclude that (up to a global phase) one has,

$$|\Psi_B\rangle_k \otimes |g_A^{\otimes N}\rangle_{k+1} \xrightarrow{\hat{\Pi}_{A^r}\hat{\Pi}_B\hat{\Pi}_{A^r}} |g_B^{\otimes N}\rangle_k \otimes |\Psi_A\rangle_{k+1} . \tag{84}$$

The proof of Eq. (75) finally follows by putting together all the identities obtained for the different sectors (again the result is obtained up to an irrelevant global phase which does not depend on the input state of the ICC).

We finally remark that an alternative (yet fully equivalent) implementation of the transformation (75) could have been realized by replacing all the π angles appearing in Eq. (76) with $-\pi$'s (with this choice the state $|\Psi; k\rangle$ will still mapped into $|\Psi; k+1\rangle$ up to a global phase). This innocent looking observation is useful to clarify why the same operators given in Eq. (77) will also induce the reverse of the mapping (75), i.e.

$$\hat{U}_{\text{shift}}|\Psi; k+1\rangle \stackrel{*}{=} |\Psi; k\rangle . \tag{85}$$

Indeed changing the sign of the π 's in Eq. (76) means taking the inverse of $\hat{\Pi}_{A^r}$, $\hat{\Pi}_B$ and $\hat{\Pi}_C$. Therefore for the case where $|\Psi; k\rangle$ is a B -type well-formed state we can write

$$\begin{aligned} \hat{\Pi}_{A^r}\hat{\Pi}_B\hat{\Pi}_C\hat{\Pi}_{A^r}|\Psi; k\rangle &\stackrel{*}{=} \hat{\Pi}_{A^r}^\dagger\hat{\Pi}_C^\dagger\hat{\Pi}_B^\dagger\hat{\Pi}_{A^r}^\dagger|\Psi; k\rangle \stackrel{*}{=} |\Psi; k+1\rangle \\ &\implies \left(\hat{\Pi}_{A^r}\hat{\Pi}_B\hat{\Pi}_C\hat{\Pi}_{A^r}\right)^2|\Psi; k\rangle \stackrel{*}{=} |\Psi; k\rangle \stackrel{*}{=} \hat{\Pi}_{A^r}\hat{\Pi}_B\hat{\Pi}_C\hat{\Pi}_{A^r}|\Psi; k+1\rangle, \end{aligned} \quad (86)$$

which proves the thesis (for A - and C -type well-formed states we can proceed similarly).

1. Explicit pulse sequence

Notice that $\hat{\Pi}_B$ induces π -pulses on all the B -type qubits (crossed and regular). A specific instance of the control parameters that allows for such operation is obtained by considering the following four step sequence $\hat{U}_B^{(4)}\hat{U}_B^{(3)}\hat{U}_B^{(2)}\hat{U}_B^{(1)}$ where

- $\hat{U}_B^{(1)}$ is induced by setting $\phi_B^{(1)} = 0$ and letting the system evolve for a time $\tau_1 = \frac{3\pi}{4}\Omega_B^{-1}$;
- $\hat{U}_B^{(2)}$ is induced by setting $\phi_B^{(2)} = \pi/2$ and letting the system evolve for a time $\tau_2 = \pi\Omega_B^{-1}$;
- $\hat{U}_B^{(3)}$ is induced by setting $\phi_B^{(3)} = \pi$ and letting the system evolve for a time $\tau_3 = \frac{\pi}{4}\Omega_B^{-1}$;
- $\hat{U}_B^{(4)}$ is induced by setting $\phi_B^{(4)} = -\pi/2$ and letting the system evolve for a time $\tau_4 = \pi\Omega_B^{-1}$;

(recall that by convention Ω_B is the Rabi frequency of the regular B -type qubits). A similar decomposition applies also to $\hat{\Pi}_C$. On the contrary $\hat{\Pi}_{A^r}$ induces π -pulses only the regular elements of the A qubits. A specific instance of the control parameters that allows for such operation is obtained by considering the following four step sequence $\hat{U}_A^{(4)}\hat{U}_A^{(3)}\hat{U}_A^{(2)}\hat{U}_A^{(1)}$ where now

- $\hat{U}_A^{(1)}$ is induced by setting $\phi_A^{(1)} = 0$ and letting the system evolve for a time $\tau_1 = \frac{\pi}{2}\Omega_A^{-1}$;
- $\hat{U}_A^{(2)}$ is induced by setting $\phi_A^{(2)} = \pi/2$ and letting the system evolve for a time $\tau_2 = \pi\Omega_A^{-1}$;
- $\hat{U}_A^{(3)}$ is induced by setting $\phi_A^{(3)} = \pi$ and letting the system evolve for a time $\tau_3 = \frac{\pi}{2}\Omega_A^{-1}$;
- $\hat{U}_A^{(4)}$ is induced by setting $\phi_A^{(4)} = -\pi/2$ and letting the system evolve for a time $\tau_4 = \pi\Omega_A^{-1}$;

(also Ω_A is the Rabi frequency of the regular A -type qubits).

C. Single-qubit gate

Referring to the previous subsection, we are able to move the interface in whatever desired position of the ladder, specifically where a χ -type crossed-qubit is positioned with χ being either equal to B or C . In order to perform a single-qubit gate, once the interface is located at the χ -type crossed-qubit, we need to send a specific global sequence of pulses involving A - and χ -type qubits. Specifically the operations needed for implementing the single-qubit gates can be realized composing control pulses that induce evolutions of the form

$$\hat{Z}_{A^r}^{\text{tot}}\hat{W}_{\chi^\times}(\theta/2; -\mathbf{n}_\perp)\hat{Z}_{A^r}^{\text{tot}}\hat{W}_{\chi^\times}(\theta/2; \mathbf{n}_\perp) \quad (87)$$

with \mathbf{n}_\perp orthogonal to \mathbf{z} and $\hat{Z}_{A^r}^{\text{tot}}$ defined in Eq. (51). Indeed thanks to the fact that the crossed B -type qubits are located on columns which are at least three columns apart from each other, when acting on $|\Psi; k\rangle$ the above transformation will effectively correspond to apply the single-qubit rotation $\hat{\mathbb{R}}(\theta, \mathbf{n}_\perp)$ on the crossed element of the ICC. The key observations here are the properties iii) and iv) of Sec. III A. Notice in fact that since $|\Psi, k\rangle$ is a well-formed state of χ -type, with k being associated with a column χ that contains a crossed term, after the action of $\hat{W}_{\chi^\times}(\theta/2; \mathbf{n}_\perp)$ it will become a well-behaved, ill-formed state,

$$\hat{W}_{\chi^\times}(\theta/2; \mathbf{n}_\perp)|\Psi; k\rangle = |\tilde{\Psi}; k\rangle := \bigotimes_{i \in \chi^\times/\text{PARA}} \hat{\mathbb{R}}_i(\theta/2, \mathbf{n}_\perp)|\Psi; k\rangle, \quad (88)$$

where in the last identity we emphasize that all the crossed χ qubits that are not in the paramagnetic area (including the one in the ICC) acquires the rotation $\hat{\mathbb{R}}_i(\theta/2, \mathbf{n}_\perp)$. Therefore under $\hat{Z}_{A^r}^{\text{tot}}$ this state will evolve as in Eq. (74) acquiring $\hat{\sigma}^{(z)}$ -gates to each of the element of the ICC, i.e. explicitly

$$\hat{Z}_{A^r}^{\text{tot}} \hat{W}_{\chi^\times}(\theta/2; \mathbf{n}_\perp) |\Psi; k\rangle = \hat{Z}_{A^r}^{\text{tot}} |\tilde{\Psi}; k\rangle = (-1)^{M'_k} \bigotimes_{\substack{i \in \chi^\times / \text{PARA} \\ j \in \text{ICC}}} \hat{\sigma}_j^{(z)} \hat{\mathbb{R}}_i(\theta/2, \mathbf{n}_\perp) |\Psi; k\rangle. \quad (89)$$

The action of $\hat{W}_{\chi^\times}(\theta/2; -\mathbf{n}_\perp)$ will be similar to what seen in Eq. (88), i.e.

$$\hat{W}_{\chi^\times}(\theta/2; -\mathbf{n}_\perp) \hat{Z}_{A^r}^{\text{tot}} \hat{W}_{\chi^\times}(\theta/2; \mathbf{n}_\perp) |\Psi; k\rangle = (-1)^{M'_k} \bigotimes_{\substack{i \in \chi^\times / \text{PARA} \\ j \in \text{ICC}}} \hat{\mathbb{R}}_i(\theta/2, -\mathbf{n}_\perp) \hat{\sigma}_j^{(z)} \hat{\mathbb{R}}_i(\theta/2, \mathbf{n}_\perp) |\Psi; k\rangle. \quad (90)$$

Since the latter is again well-behaved we can then replicate the argument of (89) to write

$$\hat{Z}_{A^r}^{\text{tot}} \hat{W}_{\chi^\times}(\theta/2; -\mathbf{n}_\perp) \hat{Z}_{A^r}^{\text{tot}} \hat{W}_{\chi^\times}(\theta/2; \mathbf{n}_\perp) |\Psi; k\rangle = (-1)^{2M'_k} \bigotimes_{\substack{i \in \chi^\times / \text{PARA} \\ j \in \text{ICC}}} \hat{\sigma}_j^{(z)} \hat{\mathbb{R}}_i(\theta/2, -\mathbf{n}_\perp) \hat{\sigma}_j^{(z)} \hat{\mathbb{R}}_i(\theta/2, \mathbf{n}_\perp) |\Psi; k\rangle. \quad (91)$$

Now the thesis follows by observing that if j corresponds to a non-crossed element of the ICC, it will experience the action of $\hat{\sigma}_j^{(z)} \hat{\sigma}_j^{(z)} = \hat{\mathbb{1}}_j$; similarly if i corresponds to a crossed element that is not in the ICC, it will experience the action of $\hat{\mathbb{R}}_i(\theta/2, -\mathbf{n}_\perp) \hat{\mathbb{R}}_i(\theta/2, \mathbf{n}_\perp) = \hat{\mathbb{1}}_i$; on the contrary if j happens to be the crossed element of the ICC it will undergo the transformation

$$\hat{\sigma}_j^{(z)} \hat{\mathbb{R}}_j(\theta/2, -\mathbf{n}_\perp) \hat{\sigma}_j^{(z)} \hat{\mathbb{R}}_j(\theta/2, \mathbf{n}_\perp) = \hat{\mathbb{R}}_i(\theta/2, \mathbf{n}_\perp) \hat{\mathbb{R}}_j(\theta/2, \mathbf{n}_\perp) = \hat{\mathbb{R}}_j(\theta, \mathbf{n}_\perp). \quad (92)$$

D. Two-qubit gate

As mentioned in the main text, to entangle two logical qubits we simply need to bring the interface at the position of the A -type crossed-qubit that connects the two logical qubits we want to entangle. Subsequently, we send a global pulse on the A -type qubits, designed to perform a 2π rotation on the crossed A -type qubits, i.e. the gate $\hat{Z}_{A^\times}^{\text{(tot)}}$ defined in Eq. (51). Thus, such qubits will acquire a (-1) phase factor if and only if the two connected B - or C -type qubits are in the ground state, realizing a controlled-phase gate (CZ). Actually, the pulse is realized to perform a 2π rotation also on the normal B -type qubits. However, this simply accounts for a global phase factor, which we discard. In summary, the transformation $\hat{Z}_{A^\times}^{\text{(tot)}}$ can be realized through a five step sequence $\hat{U}_A^{(5)} \hat{U}_A^{(4)} \hat{U}_A^{(3)} \hat{U}_A^{(2)} \hat{U}_A^{(1)}$ where

- $\hat{U}_A^{(1)}$ is induced by setting $\phi_A^{(1)} = \pi/2$ and letting evolving the system for a time $\tau_1 = \frac{\pi}{4} \Omega_A^{-1}$;
- $\hat{U}_A^{(2)}$ is induced by setting $\phi_A^{(2)} = 0$ and letting evolving the system for a time $\tau_2 = \pi \Omega_A^{-1}$;
- $\hat{U}_A^{(3)}$ is induced by setting $\phi_A^{(3)} = \pi/2$ and letting evolving the system for a time $\tau_3 = \frac{\pi}{2} \Omega_A^{-1}$;
- $\hat{U}_A^{(4)}$ is induced by setting $\phi_A^{(4)} = 0$ and letting evolving the system for a time $\tau_4 = \pi \Omega_A^{-1}$;
- $\hat{U}_A^{(5)}$ is induced by setting $\phi_A^{(5)} = \pi/2$ and letting evolving the system for a time $\tau_5 = \frac{\pi}{4} \Omega_A^{-1}$.

E. Initialization

Before we start the computation, the device is in a full ferromagnetic phase

$$|\Psi_{\text{ferro}}\rangle := |g^{\otimes N}\rangle \otimes |g^{\otimes N}\rangle \dots, \quad (93)$$

where all the qubits are in the $|g\rangle$ state. This is a stable configuration of the system Hamiltonian and, in case the ζ interaction term is positive, also corresponds to the ground state of the model. However, this is not a well-formed state and it will not react well when we apply the sequences (20). An essential ingredient of our architecture is the

ability to force transitions from $|\Psi_{\text{ferro}}\rangle$ to one of the vectors $|\Psi; k\rangle$. For this purpose we can use the following sequence of operations:

$$\hat{U}_{\text{init}} := \hat{\Pi}_{A^\times} \hat{\Pi}_{C^\times} \hat{\Pi}_{A^\times}, \quad (94)$$

with $\hat{\Pi}_{A^\times}$ and $\hat{\Pi}_{C^\times}$ the controlled π -gates defined in Eq. (76). We notice that the action of the first $\hat{\Pi}_{A^\times}$ will promote (up to a global phase) the state $|\Psi_{\text{ferro}}\rangle$ in a vector $|\Psi'_{\text{ferro}}\rangle$ where all the crossed A -type qubits are in the $|e\rangle$ state keeping all the others in the $|g\rangle$ state. When acting on such configuration with $\hat{\Pi}_{C^\times}$ we will induce a $|g\rangle \rightarrow |e\rangle$ transition on the elements of the first column of the device since they are crossed C -type qubits with all neighbouring qubits in the ground state. Notice that the other crossed C -type qubits have instead a crossed A -type qubit in the $|e\rangle$ state which blocks such transition. The new state $|\Psi''_{\text{ferro}}\rangle$ has hence all the qubits of the first C column and all the crossed A -type elements in the $|e\rangle$ state and all the remaining elements in the $|g\rangle$ state. When we finally act with the second $\hat{\Pi}_{A^\times}$ operation, all the crossed elements of A will return to $|g\rangle$ since all their neighbouring qubits are still in the $|g\rangle$ state, i.e.

$$\begin{aligned} |\Psi_{\text{ferro}}\rangle &\xrightarrow{\hat{\Pi}_{A^\times}} |\Psi'_{\text{ferro}}\rangle := \left(\otimes_{i \in A^\times} |e_i\rangle \right) \left(\otimes_{i' \notin A^\times} |g_{i'}\rangle \right) \\ &\xrightarrow{\hat{\Pi}_{C^\times}} |\Psi''_{\text{ferro}}\rangle := \left(\otimes_{j \in C_1} |e_j\rangle \right) \left(\otimes_{i \in A^\times} |e_i\rangle \right) \left(\otimes_{i' \notin A^\times \cup C_1} |g_{i'}\rangle \right) \\ &\xrightarrow{\hat{\Pi}_{A^\times}} |\Psi'''_{\text{ferro}}\rangle := \left(\otimes_{j \in C_1} |e_j\rangle \right) \left(\otimes_{i' \notin C_1} |g_{i'}\rangle \right), \end{aligned} \quad (95)$$

where C_1 represents the set of qubits of the first column of the device. Notice that the final state of the transformation corresponds to the well-formed state $|\Psi_0; 3\rangle$ where the ICC is located in the first B column of the processing area, and a logical state $|\Psi_0\rangle := |g^{\otimes N}\rangle$. From this state, we can start the computation moving the ICC back and forth on the processing area to apply any desired quantum gate.

It is worth mentioning that an alternative approach to realize the mapping from $|\Psi_{\text{ferro}}\rangle$ to $|\Psi_0; 3\rangle$, is to include an extra dedicated control line $V_{\text{init}}(t)$ that acts selectively on the first column of the device as shown in panel (a) of Fig. 3. Such term contributes to the Hamiltonian of the model via the following time-dependent term

$$\hat{H}_{\text{init}}(t) := \sum_{i \in C_1} \frac{\hbar \Omega_{\text{init}}(t)}{2} \left(e^{i\phi_{\text{init}}(t)} |g_i\rangle \langle e_i| + \text{H.c.} \right), \quad (96)$$

where $\phi_{\text{init}}(t)$ and $\Omega_{\text{init}}(t)$ are the associated control functions. Therefore tailoring the phase, the Rabi frequency, and the duration τ_{init} of the control line we can induce the evolution $\hat{\Pi}_{C_1} := \hat{W}_{C_1}(\pi; \mathbf{x}) = \prod_{i \in C_1} \left[\hat{\mathbf{1}}_i \otimes \hat{Q}_{(i)} - i\hat{\sigma}_i^{(x)} \otimes \hat{P}_{(i)} \right]$, which indeed allow us to realize the required mapping.

F. Read-out

At the end of the computation, we read out the logical state of the ICC by moving it to the rightmost element of the process unit (i.e., the B - or C -type column of the read-out area) using the transformations \hat{U}_{shift} . Despite it is theoretically possible to measure the logical state of the ICC column while it is inside the process area, we prefer not to do this. Such an approach would inevitably require local addressing of the elements within the column, which contradicts the fundamental principles of our architecture. Notice also that the scheme presented in Fig. 1 of the main text represents the minimal setting that allows for a separation between the processing area and the read-out column. If we need to increase this separation, it can be easily accomplished by adding an extra sequence of columns in the read-out area, see panel (b) of Fig. 3.

IV. NUMERICAL SIMULATIONS

In this Section we perform exact numerical simulations to test the $e-e$ blockade regime (Sec. IV A) and the validity of the protocol allowing the motion of logical states (Sec. IV B) and the protocol realizing the Hadamard (single-qubit) gate (Sec. IV C).

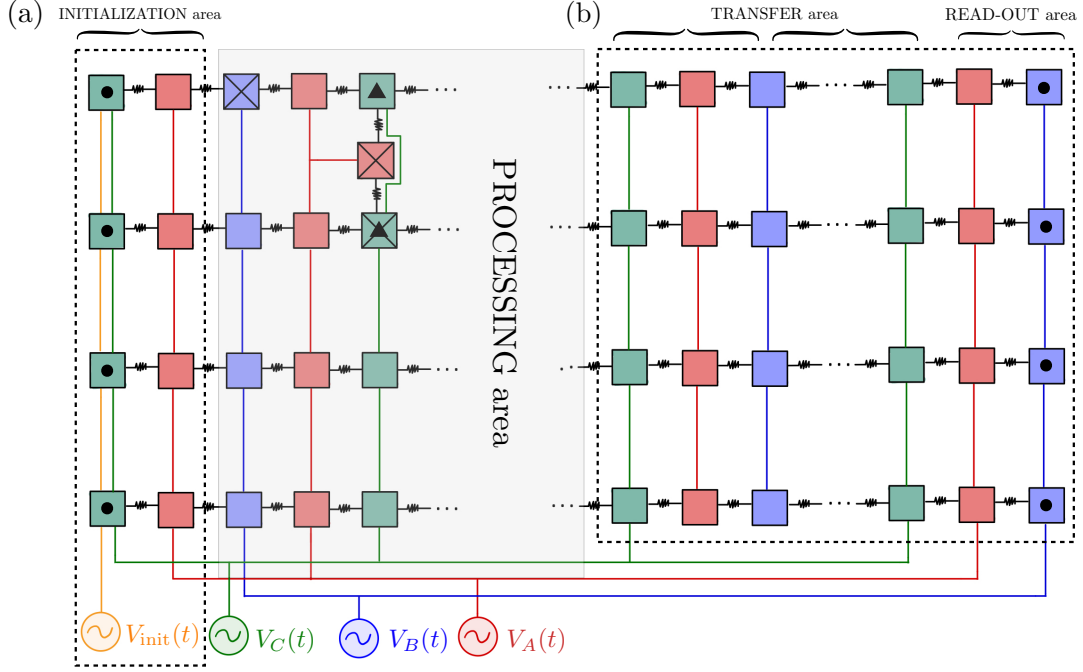


FIG. 3: In panel (a) we present an alternative realization of the initialization area with respect to the design of Fig. 1 of the main text. Here the first column is selectively addressed by an extra control line $V_{\text{init}}(t)$ (continuous golden line) which acts independently from $V_A(t)$ and $V_B(t)$. Notice that in this case we do not need the element of the first column to be crossed. In panel (b) we show how to use extra columns (transfer area) to outdistance the last column of the read-out area from the processing area.

A. Testing the blockade regime

In order to test our proposal for reaching the blockade effect, we simulate the dynamic evolution of a system made of three qubits, e.g. the chain A_1BA_2 , under the Hamiltonian (7). Here, the drive (8) controls only the B -type qubit in the middle of the chain, whose natural frequency is ω_B . In Fig. 4 the dynamics of the B -type qubit is shown. As explained (e.g. see Fig. 2(a) of the main text), in order to reach the e - e blockade, we must drive the B -type qubit with an off-resonant pulse of frequency $\omega_d = \omega_B - 2\zeta$. In the following, we simulate the system starting from three different initial configurations: $|ggg\rangle$, $|gge\rangle$ and $|gg+\rangle$ [S12]. The plots of Fig. 4, from left to right, show the population P_e of the excited state over the π -pulse dynamics for a three-qubit chain. It is easy to see that the desired blockade regime is reached.

B. Checking the motion of the interface

By using the protocol explained in the previous Section, we now perform numerical simulations in order to check the correct motion of the interface for one single row of alternating A , B - and C - type qubits. There are no crossed qubits in the system. Firstly, we initialize the state of the qubits and then we allow the system to evolve under the total Hamiltonian (19). Secondly, we perform the protocol defined above in Sec. III B. The results are shown in Fig. 5 where the interface is shifted from left to right.

C. Gate Fidelity

One method for evaluating the efficacy of our protocol is to compute the average gate fidelity, denoted by $\langle \mathcal{F} \rangle$. It is possible that errors are introduced due to the blockade being exact only in the $\eta_{\text{BR}} \gg 1$ limit. In particular, using a 5-qubits row, we simulate the pulse sequence which performs a Hadamard gate on the logical qubit at the position of the crossed B -type qubit, see Sec. III C. The average is calculated by averaging over approximately $\mathcal{O}(10^2)$ random

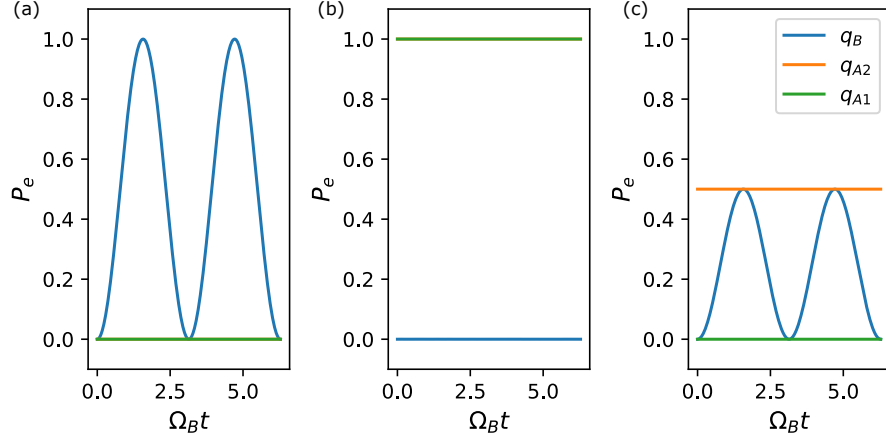


FIG. 4: Numerical simulation for a three-qubit chain where the B -type qubit is the only driven by an external π -pulse. Here P_e denotes the population of the excited state of each qubit and time is measured in units of Ω_B . The driven qubit is denoted as q_B and is initialised in the ground state. Its neighbours are q_{A1} and q_{A2} . To reach the e - e blockade, pulses of frequency $\omega_d = \omega_B - 2\zeta$ drive the B -type qubit of the chain. The plots in the figure show the population P_e after the effect of the driving pulse. (a) The qubits at the extremes of the chain are initialised in the ground state, so the dynamics of the driven qubit is not blocked. (b) The external qubits are both in the excited state, resulting in blockade dynamics for the driven B -type qubit. (c) The qubit on the right of the chain, q_{A2} , is initialised in the superposition $|+\rangle$, while the qubit q_{A1} is in the ground state. With this initial configuration, we expect the driven qubit to reach the $|+\rangle$ state, since it is “half” blocked.

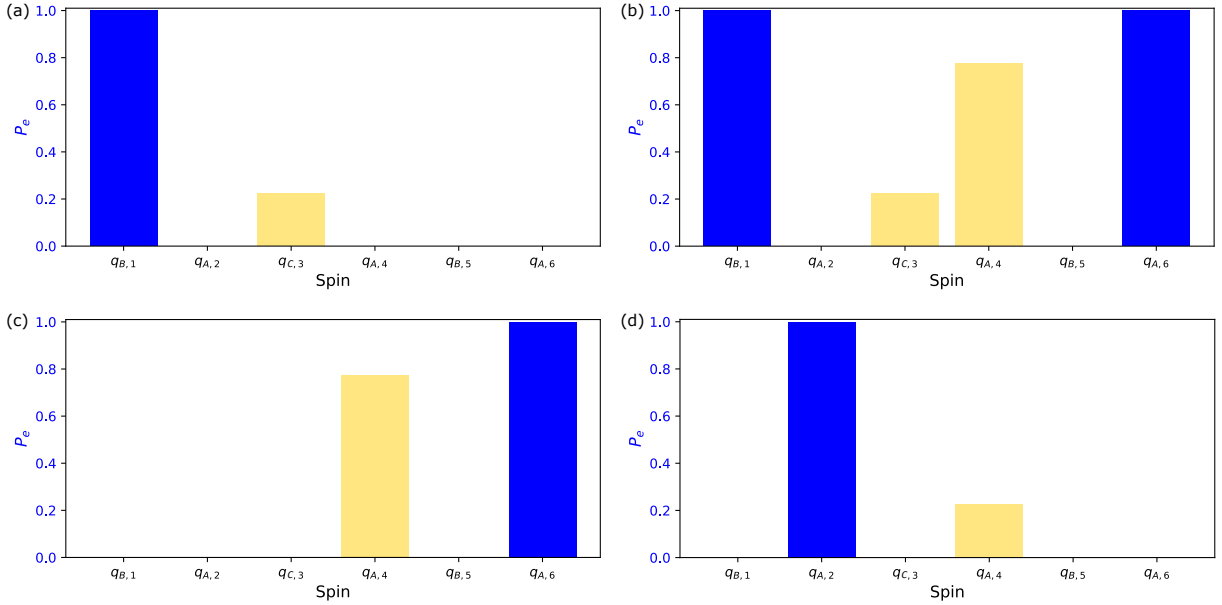


FIG. 5: Time evolution for a single row of 6 regular qubits. The bars indicate the probability P_e of finding the two-level system in the excited state. The χ -type qubits in the row are denoted as $q_{\chi,i}$, where $i \in (1,6)$ stands for the spatial position coordinate in the row. (a) Initial state of the system, with the $i = 3$ qubit as the logic one. The interface is colored in yellow. (b) State of the system after the $\hat{\Pi}_A$ pulse. Here the third and fourth qubits are entangled and the interface is shared. (c) State of the system after the $\hat{\Pi}_B \hat{\Pi}_C \hat{\Pi}_A$ pulse. (c) Final state, after the entire pulse sequence $\hat{U}_{\text{shift}} = \hat{\Pi}_A \hat{\Pi}_B \hat{\Pi}_C \hat{\Pi}_A$. The logical qubit is now at position $i = 4$.

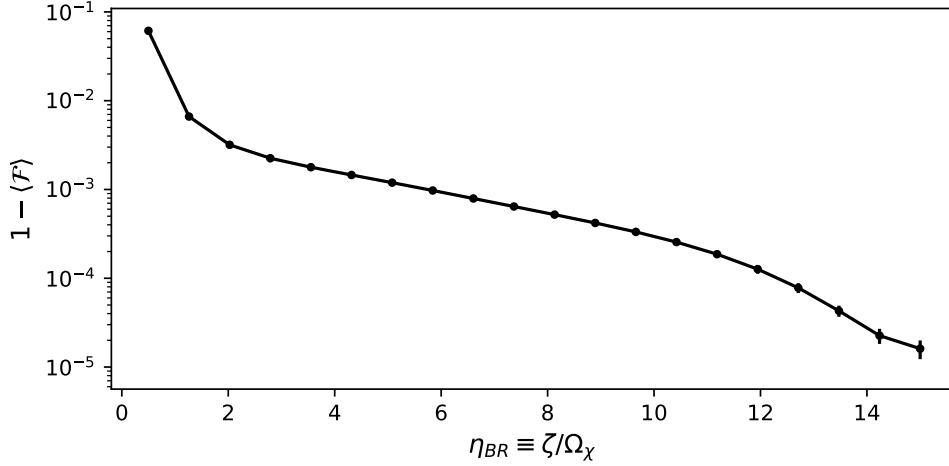


FIG. 6: $1 - \langle \mathcal{F} \rangle$ as a function of the ratio between the ZZ coupling ζ and the Rabi frequency Ω_χ . Note that $\eta_{BR} = 5$ is sufficient to reach a 99.9% gate fidelity.

initializations of the crossed qubit state. For each initialization, the fidelity is computed according to the formula [S11]

$$\mathcal{F}(\hat{\rho}_{\text{target}}, \hat{\rho}_{\text{exp}}) = \text{Tr} \left(\sqrt{\sqrt{\hat{\rho}_{\text{target}}} \hat{\rho}_{\text{exp}} \sqrt{\hat{\rho}_{\text{target}}}} \right), \quad (97)$$

where the density matrix of the system after the application of a perfect Hadamard gate on the crossed qubit is denoted by $\hat{\rho}_{\text{target}}$, while the density matrix we get after performing the pulse sequence in our system is represented by $\hat{\rho}_{\text{exp}}$. The result is presented in Fig. 6, in which the average gate fidelity is plotted as a function of the ratio between the qubit-qubit coupling constant, ζ , and the Rabi frequency, Ω_χ , with $\chi = A, B, C$. From the graph, it is evident that a ratio of 5 is sufficient to achieve a gate fidelity of 99.9%.

-
- [S1] P. Krantz, M. Kjaergaard, F. Yan, T. P. Orlando, S. Gustavsson, and W. D. Oliver, A quantum engineer's guide to superconducting qubits, *Appl. Phys. Rev.* **6**, 021318 (2019).
- [S2] A. Blais, A. L. Grimsmo, S. M. Girvin, and A. Wallraff, Circuit quantum electrodynamics, *Rev. Mod. Phys.* **93**, 025005 (2021).
- [S3] L. DiCarlo, J. M. Chow, J. M. Gambetta, L. S. Bishop, B. R. Johnson, D. I. Schuster, J. Majer, A. Blais, L. Frunzio, S. M. Girvin, and R. J. Schoelkopf, Demonstration of two-qubit algorithms with a superconducting quantum processor, *Nature* **460**, 240–244 (2009).
- [S4] M. Kounalakis, C. Dickel, A. Bruno, N. K. Langford, and G. A. Steele, Tuneable hopping and nonlinear cross-Kerr interactions in a high-coherence superconducting circuit, *npj Quantum Inf* **4**, 38 (2018).
- [S5] S. E. Rasmussen, K. Groenland, R. Gerritsma, K. Schoutens, and N. T. Zinner, Single-step implementation of high-fidelity n -bit Toffoli gates, *Phys. Rev. A* **101**, 022308 (2020).
- [S6] A. J. Baker, G. B. P. Huber, N. J. Glaser, F. Roy, I. Tsitsilin, S. Filipp, M. J. Hartmann, Single shot i -Toffoli gate in dispersively coupled superconducting qubits, *Appl. Phys. Lett.* **120**, 054002 (2022).
- [S7] F. Yan, P. Krantz, Y. Sung, M. Kjaergaard, D. L. Campbell, T. P. Orlando, S. Gustavsson, and W. D. Oliver, Tunable Coupling Scheme for Implementing High-Fidelity Two-Qubit Gates, *Phys. Rev. Appl.* **10**, 054062 (2018).
- [S8] Y. Sung, *et al.*, Realization of High-Fidelity CZ and ZZ-Free iSWAP Gates with a Tunable Coupler, *Phys. Rev. X*, **11**, 021058 (2021).
- [S9] M. C. Collodo, *et al.*, Implementation of Conditional Phase Gates Based on Tunable ZZ Interactions, *Phys. Rev. Lett.* **125**, 240502 (2020).
- [S10] F. Arute, *et al.*, Quantum supremacy using a programmable superconducting processor, *Nature* **574**, 505 (2019).
- [S11] M. A. Nielsen and I. L. Chuang, *Quantum Computation and Quantum Information* (Cambridge University Press, Cambridge, 2010).
- [S12] The $|+\rangle$ state denotes the Hadamard state $(|g\rangle + |e\rangle)/\sqrt{2}$.
- [S13] F. Cesa and H. Pichler, Universal Quantum Computation in Globally Driven Rydberg Atom Arrays, *Phys. Rev. Lett.* **131**, 170691 (2023).